Theses and Dissertations

Spring 2012

Striated muscle action potential assessment as an indicator of cellular energetic state

Colin Michael-Lee Burnett
University of Iowa

Recommended Citation

Burnett, Colin Michael-Lee. "Striated muscle action potential assessment as an indicator of cellular energetic state." MS (Master of Science) thesis, University of Iowa, 2012.
http://ir.uiowa.edu/etd/2830.

STRIATED MUSCLE ACTION POTENTIAL ASSESSMENT AS AN INDICATOR

OF CELLULAR ENERGETIC STATE

by

Colin Michael-Lee Burnett

A thesis submitted in partial fulfillment
of the requirements for the Master of
Science degree in Biomedical Engineering
in the Graduate College of
The University of Iowa

May 2012

Thesis Supervisor: Assistant Professor Denice M. Hodgson-Zingman

Graduate College
The University of Iowa
Iowa City, Iowa

CERTIFICATE OF APPROVAL

_____

MASTER'S THESIS

_____

This is to certify that the Master's thesis of

Colin Michael-Lee Burnett

has been approved by the Examining Committee
for the thesis requirement for the Master of Science
degree in Biomedical Engineering at the May 2012 graduation.

Thesis Committee: _____
                        Denice M. Hodgson-Zingman, Thesis Supervisor

                  _____
                        Edwin L. Dove

                  _____
                        Joseph M. Reinhardt

To Sarah

ACKNOWLEDGMENTS

ABSTRACT

Action potentials of striated muscle are created through movement of ions through membrane ion channels. ATP-sensitive potassium (K_{ATP}) channels are the only known channels that are gated by the intracellular energetic level ([ATP]/[ADP] ratio). K_{ATP} channels are both effectors and indicators of cellular metabolism as part of a negative feedback system. Decreased intracellular energetic level alters the gating of K_{ATP} channels, which is reflected in alterations of the action potential morphology. These changes protect the cell from exhaustion or injury by altering energy-consuming processes that are driven by membrane potential. Assessing the effects of K_{ATP} channel activation on resting membrane potential and action potential morphology, and the relationship to cellular stress is important to the understanding of normal cellular function. To better understand how muscle cells adapt to energetic stress, the monophasic action potential (MAP) electrode and floating microelectrode were used to record action potentials in intact hearts and skeletal muscles, respectively. Intact organs provide a more physiological environment for the study of energetics and membrane electrical phenomena. Utilizing these techniques, a stress on the intracellular energetic state resulted in greater and faster shortening of the duration of cardiac action potentials, and hyperpolarization of the membrane of skeletal muscle in a K_{ATP} channel dependent manner. Motion artifacts are a limitation to studying transmembrane action potentials, but the MAP and floating microelectrode techniques uniquely allow for reading of action potential morphology uncoupled from motion artifacts. The use of the floating microelectrode in skeletal muscles is a novel approach that provides previously unavailable data on skeletal muscle membrane potentials *in situ*.

TABLE OF CONTENTS

LIST OF FIGURES

LIST OF SYMBOLS

F   Faraday's constant (96,485 C mol^{-1})

P_x Permeability constant of ion X

R   Gas constant (8.314 J K^{-1} mol^{-1})

T   Temperature (K)

V_m Membrane potential

V_{Ca} Reversal potential for calcium ions

V_{Cl} Reversal potential for chloride ions

V_K Reversal potential for potassium ions

V_{Na} Reversal potential for sodium ions

[X]   Molarity; concentration of X (M=mol L^{-1})

$[X]_i$ Molarity inside of a cell

$[X]_o$ Molarity outside of a cell

z   Elemental charge of an ion (e.g., monovalent cation is +1)

LIST OF ABBREVIATIONS

αMHC	Alpha-myosin heavy chain
ABCC	ATP binding cassette, sub-family C
ABCC8	ABCC, member 8; gene that encodes SUR1
ABCC9	ABCC, member 9; gene that encodes SUR2A and SUR2B
ADP	Adenosine diphosphate
Ag/AgCl	Silver wire coated with silver chloride
Ala	Alanine
AP	Action potential
APD	Action potential duration, milliseconds
APD_{90}	APD at 90% width, milliseconds
ΔAPD_{90}	Change between two APD_{90} values, milliseconds
ATP	Adenosine triphosphate
CX1	Chicken β-actin
DAQ	Data acquisition
ECC	Excitation-contraction contraction
ECG	Electrocardiogram
EDL	Extensor digitorum longus
eGFP	Enhanced green fluorescent protein
EMG	Electromyogram
EPP	End-plate potential
FM	Frequency modulation
FME	Floating microelectrode
GHK	Goldman-Hodgkin-Katz equation
GFP(+)	eGFP-expressing mouse; refers to Tg[CX1-eGFP-K_{ir}6.1AAA]
Gly	Glycine

INN   International Nonproprietary Name

K_{ATP} ATP-sensitive potassium channels

K_{ir} Inwardly-rectifying potassium channels

$K_{ir}6.1AAA$

            Mutant $K_{ir}6.1$ with Ala-Ala-Ala replacing Gly-Phe-Gly

MAP   Monophasic action potential

KCNJ   Potassium inwardly-rectifying channel, sub-family J

KCNJ8   KCNJ, member 8; gene that encodes $K_{ir}6.1$

KCNJ11   KCNJ, member 11; gene that encodes $K_{ir}6.2$

ME   Microelectrode

MgADP   Magnesium ADP

MyoD   Myogenic differentiation 1; a transcription factor

Phe   Phenylalanine

PTFE   Polytetrafluoroethylene ("Teflon")

QT_c Heart rate-corrected QT interval

sEMG   Surface electromyogram

SERCA   Sarco/endoplasmic reticulum calcium-ATPase

SIU   Stimulus isolation unit

SR   Sarcoplasmic reticulum

SUR   Sulfonylurea receptor; SUR1, SUR2A, SUR2B

TA   Tibialis anterior muscle

TG   Transgenic

Tg[CX1-eGFP-$K_{ir}6.1AAA$]

            TG mouse with CX1 promoter, eGFP, and $K_{ir}6.1AAA$

Tg[αMHC-Cre]

            TG mouse with the αMHC promoter and Cre recombinase

Tg[αMHC-K$_{ir}$6.1AAA]

TG mouse with the CX1-eGFP-K$_{ir}$6.1AAA and αMHC-Cre

Tg[MyoD-Cre]

TG mouse with the MyoD promoter and Cre recombinase

Tg[MyoD-K$_{ir}$6.1AAA]

TG mouse with the CX1-eGFP-K$_{ir}$6.1AAA and MyoD-Cre

USAN United States Adopted Name

WT Wild type

CHAPTER 1

INTRODUCTION

The metabolic pathways of cells have a long evolutionary history of controlling energy and its use. Energy is required for life and because energy is generally scarce, proper control is essential. However, not all cells function equally as some have low metabolic demands like chondrocytes and some have high metabolic demands like striated muscle. Striated muscle includes two of the three muscle types: skeletal and cardiac muscle.

Skeletal muscle makes up a significant proportion of the human body. It can consume 20-73% of the cardiac output (Widmaier, Raff et al. 2008) and, even under sedentary conditions, skeletal muscle requires 7-10% of daily energy use (Barness, Opitz et al. 2007). Basal level can increase 20-100 times to meet demands during strenuous exercise (Spriet and Hargreaves 2006). Skeletal muscle is the only muscle type that is under voluntary control and the only type tasked with mobility.

The second type of striated muscle is cardiac muscle and it is only found in the heart. The heart beats continuously throughout life and has adapted to this task. Despite being the organ responsible for bulk movement of nutrients and waste, the heart consumes only 4% of the cardiac output under both sedentary and exercise conditions (Widmaier, Raff et al. 2008). Since the heart beats continuously, the control of energy is paramount. If the heart is inadequately perfused, then the cardiac output can be disrupted, which can lead to severe cellular injury and/or death for those tissues dependent on constant perfusion (e.g., nervous tissue).

Intolerance by critical tissues to gaps in perfusion has evolutionarily driven metabolic systems to be conservative and pessimistic thereby retaining excess energy. Primarily, energy is retained in white adipocytes in the form of triglycerides that leads to

both hypertrophy and hyperplasia of white adipocytes (de Ferranti and Mozaffarian 2008). This excessive accumulation leads to being overweight and, eventually, to being obese. Currently, many nations face what is often called an epidemic of obesity in both adults and children (Barness, Opitz et al. 2007) regardless of income level (Popkin, Adair et al. 2012). In the United States alone, the prevalence of obesity has increased year over year from 1986 (Sturm 2007).

The consequences of obesity are diverse (Haslam and James 2005; Anandacoomarasamy, Caterson et al. 2008): insulin resistance, glucose intolerance, type 2 diabetes mellitus, hypertension, coronary heart disease, stroke, sleep apnea, cancer (breast, colon, endometrium, kidney, esophagus), hirsutism, polycystic ovary syndrome, pre-eclampsia, gestational diabetes, arthritis, hyperuricemia, gout, fatty liver disease, gallstones, depression, rheumatoid arthritis, osteoarthritis (knee, hip, hand), low back pain, diffuse idiopathic skeletal hyperostosis, carpal tunnel syndrome, and osteoporosis. Caloric reduction dieting has been a failure, and pharmacotherapies are few in number, insufficient as stand-alone treatments, and have historical objections from low efficacy drug cocktails and drug withdrawal (Haslam and James 2005). This has lead to an increase use of bariatric surgery in both adults and children (Solomon and Dluhy 2004). Bariatric surgery has a 25-30% weight loss over 10 years but long-term change in mortality is unknown (Sjostrom, Lindroos et al. 2004). Therefore, another approach is warranted.

From one perspective, obesity is the result of the body's evolutionary success at energy control in energy-scarce environments. Greater energy intake than is expended creates an energy imbalance that is universally recognized as the root cause of obesity. Energy intake can be altered by bariatric interventions and "dieting." Exercise is a common means to modify energy expenditure, but the cultural and technological driving force of a more sedentary lifestyle is reducing average exercise levels to a point that practically any exercise is beneficial (Blair, Kohl et al. 1995). By looking at the energy

imbalance simply as intake less expenditure ignores the most prominent member of this relationship: the body. After all, it is the efficiency of the body that has led to retention of excess energy. Perhaps a viable alternative — especially in cases where obesity has serious health consequences — is to decrease bodily energy efficiency.

One historic attempt of note is that of 2,4-dinitrophenol (DNP). DNP was used in the 1930's (Tainter, Cutting et al. 1934) as a way to decrease the efficiency of cells by reducing the proton gradient in mitochondria that drives ATP synthesis. Although known to be toxic and lethally hyperthermic at high doses, moderate doses were shown to be effective at increasing energy consumption. However, DNP has undesirable side effects (e.g., cataracts) that led the FDA to removed DNP from the market in 1938 (Harper, Dickinson et al. 2001). Mitochondrial uncoupling is of continued interest decades later, but some organs (e.g., heart, brain) may experience undesirable consequences as a result of systemic mitochondrial uncoupling (Harper, Dickinson et al. 2001).

As one of the largest consumers of energy, a target of decreasing efficiency could be skeletal muscle. Instead of targeting mitochondrial uncoupling in skeletal muscle, perhaps disruption of the ATP-sensitive potassium (K_{ATP}) channels would lead to a more systemically tolerated therapy. K_{ATP} channels are the only known membrane channels that are gated by the cell's intracellular energetic state. More specifically, K_{ATP} channels act as a negative feedback loop to reduce energy consumption as the energetic state is taxed.

To target K_{ATP} channels, it is first necessary to understand the bioenergetics of striated muscle; second, to understand how to manipulate it; and, third, to be able to manipulate it. The current state of understanding of striated muscle does not paint a complete enough picture of its bioenergetics. The involvement of K_{ATP} channels in cellular bioenergetics through their function in the plasma membrane has been understood for decades. As active members of the plasma membrane, participation of

K_{ATP} channels in the morphology of action potentials may provide a useful indicator to further the understanding of the bioenergetics of striated muscle.

CHAPTER 2

BACKGROUND

Like all cells, myocytes have a phospholipid bilayer called the plasma membrane. This membrane contains numerous proteins with an equally large number of functions. Some of these proteins are responsible for movement of ions that creates an electrical potential between the intracellular and extracellular spaces. These proteins are called ion channels, transporters, and exchangers. Some proteins make the membrane electrochemically excitable and the membrane is said to be an excitable membrane. Ion channels are commonly gated through ligands or through the membrane potential. A third gating mechanism is through a change in the intracellular energetic state. The only known channels co9-ntrolled in this manner are a family of inwardly-rectifying potassium channels (K_{ir}) called ATP-sensitive potassium (K_{ATP}) channels.

2.1 Excitable Membranes

2.1.1 Membrane Potential

In electrical circuits, potentials are created through separation of electrons, and currents are created through movement of electrons. In general in cells, potentials and currents are not carried by electrons but through chemical ions (notable exception is the electron transport chain in mitochondria). Using the plasma membrane as a barrier, ions can be separated on different sides to create a membrane potential. The membrane potential assumes a zero reference on the extracellular side and can be approximated by the Goldman-Hodgkin-Katz (GHK) voltage equation on an infinite, planar membrane at a steady-state (Fraser and Huang 2007).

$$V_m = 1000 \left[\frac{RT}{F \log_{10} e} \log_{10} \frac{\sum P_X [X^+]_o + \sum P_Y [Y^-]_i}{\sum P_X [X^+]_i + \sum P_Y [Y^-]_o} \right]$$

$$V_m = (61.5) \log_{10} \frac{\sum P_X [X^+]_o + \sum P_Y [Y^-]_i}{\sum P_X [X^+]_i + \sum P_Y [Y^-]_o}$$

where R is the ideal gas constant (8.314 J K^{-1} mol^{-1}), T is the temperature in Kelvin (can be assumed to be $37°C=310$ K as done for the second equation), and F is Faraday's constant ($96,485$ C mol^{-1}). Both of these equations yield millivolts. Cations, denoted with X, and anions, denoted with Y, have opposite charges and have different membrane permeability (denoted by P_X and P_Y). Increasing the numerator makes the membrane potential more positive, and increasing the denominator makes the membrane potential more negative. For example, increasing the intracellular potassium (K^+) concentration would make the membrane potential more negative. (For derivation of the GHK equation, see 2.3 of (Fraser and Huang 2007).)

As an example, if the following assumptions are made for permeabilities and ion concentrations of skeletal muscle: $P_K=100$, $[K^+]_i=150$, $[K^+]_o=4.5$; $P_{Na}=1$, $[Na^+]_i=12$, $[Na^+]_o=145$; $P_{Ca}\approx0$, $[Ca^{2+}]_o=1.8$, $[Ca^{2+}]_i=0.0002$; and $P_{Cl}=1000$, $[Cl^-]_i=4.2$, $[Cl^-]_o=116$. The permeability of calcium is extremely small at resting membrane potentials so that it has negligible effects on V_m.

$$V_m = (61.5) \log_{10} \left(\frac{100 \cdot 4.5 + 1 \cdot 145 + 0 \cdot 1.8 + 1000 \cdot 4.2}{100 \cdot 150 + 1 \cdot 12 + 0 \cdot 0.0002 + 1000 \cdot 116} \right) = -88.4 \text{ mV}$$

If the ions of the GHK equation are all eliminated but one, then the GHK equation reduces to the Nernst potential equation where z is the elementary charge of the ion.

$$V_m = \frac{RT}{zF} \log_e \frac{[X^+]_o}{[X^+]_i} = \left(\frac{61.5}{z}\right) \log_{10} \frac{[X^+]_o}{[X^+]_i}$$

When used for a single ion, the voltage calculated is called the reversal potential and is the voltage in which there is no net ion flow. When the membrane potential is not at the reversal potential for an ion, then changes in the permeability through opening or closing of ion channels will change the membrane potential.

Continuing the above example for potassium (K^+), sodium (Na^+), calcium (Ca^{2+}), and chloride (Cl^-), the reversal potentials are calculated below.

$$V_K = (61.5) \log_{10} \frac{4.5}{150} = -93.7 \text{ mV}$$

$$V_{Na} = (61.5) \log_{10} \frac{145}{12} = +66.6 \text{ mV}$$

$$V_{Ca} = \left(\frac{61.5}{2}\right) \log_{10} \frac{1.8}{0.0002} = +121.6 \text{ mV}$$

$$V_{Cl} = (61.5) \log_{10} \frac{4.2}{116} = -88.6 \text{ mV}$$

For this example membrane, the resting membrane potential is different than the reversal potential for any of the four ions (V_K, V_{Na}, V_{Ca}, V_{Cl}). Increasing the extracellular-to-intracellular ratio would increase the reversal potential for potassium, sodium, and calcium, but would decrease for chloride because chloride is an anion.

2.1.2 Action Potential

The membrane potential is a stable steady state, not equilibrium, of ion currents. In excitable membranes, this steady state can be disrupted with an action potential. The action potential morphology is varied and determined by the unique set of channels in the cell. There are two action potential morphologies of particular interest here. One is the

non-myogenic action potential of a ventricular myocyte (hereafter referred to simply as "cardiac action potential"); the second is of skeletal muscle sarcolemma. These action potentials have some characteristics:

- The baseline membrane potential before and after the action potential is at a steady state voltage. (This is not true, for example, for the cardiac sinoatrial node.)

- A threshold voltage the membrane must depolarize to in order to trigger an action potential.

- A rising phase where the membrane potential becomes more positive and typically exceeds 0 mV. This is called depolarization and overshoot, respectively.

- A falling phase where the membrane potential becomes negative once again. This is called repolarization.

Additionally, the cardiac action potential has a plateau phase between depolarization and repolarization that extends the action potential duration by two orders of magnitude compared to skeletal muscle. The plateau phase arises from counter-flows of potassium efflux and calcium influx currents. Thus, if the potassium current were larger then the plateau phase would be shorter whereas a smaller potassium current would lengthen the plateau.

The cardiac action potential morphology has garnered considerable attention to the extent that each phase has been identified, numbered, and assigned therapeutic drugs that affect that phase (Figure 1). No such classifications of skeletal muscle action potentials exist.

In both cardiac and skeletal muscle, the action potential is the first part — the excitation — in the excitation-contraction coupling (ECC) that couples contraction to the excitation of the membrane. The action potential leads to an increase in intracellular calcium concentration and an efflux of calcium out of the sarcoplasmic reticulum. Calcium acts as a secondary messenger and is the link between excitation and

contraction. In striated muscle, the calcium binds to the C component of the troponin complex, which moves the tropomyosin to expose the myosin-binding site on actin. With sufficient ATP present then cross-bridge cycling produces tension along the length of the myofibril. This continues until the concentration of calcium drops due to active pumping of calcium back into the sarcoplasmic reticulum by the sarco/endoplasmic reticulum calcium-ATPase (SERCA).
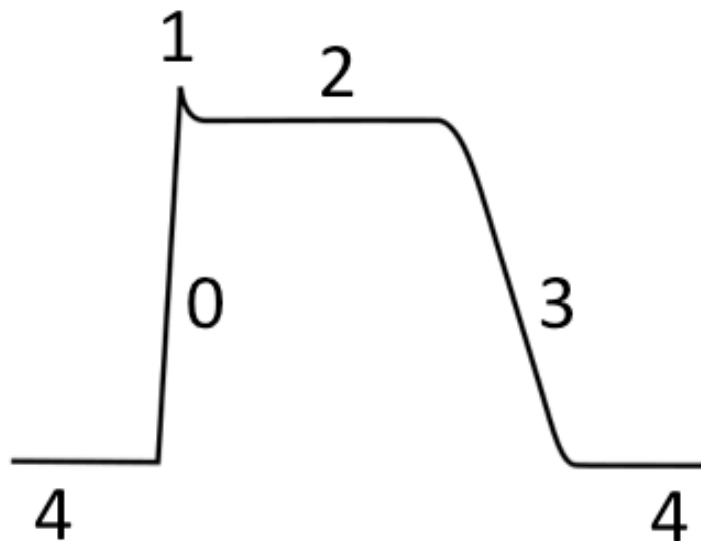
Figure 1.   The five phases of the cardiac action potential: 4=baseline, 0=depolarization, 1=small repolarization, 2=plateau, and 3=repolarization.

Taking a step back, the creation of the action potential is different between cardiac and skeletal muscle. In cardiac muscle, myocytes are connected in series and parallel to each other through intercalated discs and the intracellular spaces are connected through gap junctions. Gap junctions permit ionic currents to transmit action potentials through cardiac muscle in waves. In skeletal muscle, each individual myocyte is

innervated by a motor neuron and the intracellular spaces are not connected. Motor neurons release acetylcholine vesicles that create end-plate potentials (EPP) on the myocyte that lead to depolarization of the end plate and the sarcolemma, and creation of an action potential.

Many different ion channels participate in both the membrane potential and the action potential. A particular combination of these channels leads to cell-specific behavior of the membrane and is why, for example, the cardiac sinoatrial node behaves differently from a neuron. One subfamily of potassium channels is the ATP-sensitive potassium (K_{ATP}) channel and this subfamily alters the membrane with respect to changes in the cellular energetic state.

2.2 K_{ATP} Channels

Potassium channels are a diverse group of channels and one subfamily of potassium channels are the "inwardly rectifying" potassium channels (designated K_{ir}). There are eight subfamilies of K_{ir} and they are designated $K_{ir}1$ through $K_{ir}8$ (Hille 2001). Within each subfamily channels are designated as $K_{ir}X.Y$ in the order they were identified (e.g., $K_{ir}6.1$ then $K_{ir}6.2$). What makes the K_{ir} family "inwardly rectifying" is that they conduct less during depolarization than hyperpolarization. Some are more strongly rectifying and conduct very little for positive membrane potential (e.g., $K_{ir}2$), and some are weakly rectifying (e.g. $K_{ir}6$). Although labeled as inwardly rectifying, these channels typically have an efflux of potassium out of the cell due to $V_K < V_m$. These channels, like potassium channels in general, are recognized as "stabilizing" the plasma membrane by making V_m more negative and harder to reach the thresholds of voltage-gated channels. During an action potential, increased K_{ATP} channel current would also have an influence towards repolarization, thus shortening action potential duration in the case of cardiac action potentials, possibly reducing action potential amplitude and resting membrane potential in skeletal muscle.

One subfamily of K_{ir} is gated by ATP and is called ATP-sensitive potassium channels and is given the systematic designation of $K_{ir}6$. These channels were originally discovered in cardiac muscle (Noma 1983) and there are currently two channels in this subfamily: $K_{ir}6.1$ and $K_{ir}6.2$. The K_{ATP} channel construction is a hetero-octamer of four $K_{ir}6$ subunits and four regulatory SUR subunits with 1:1 stoichiometry. The SUR unit is a sulfonylurea receptor and is named for its affinity to sulfonylureas (e.g., glyburide).

$K_{ir}6.1$ is encoded by the *KCNJ8* gene (potassium inwardly-rectifying channel subfamily J member 8) and $K_{ir}6.2$ is encoded by the *KCNJ11* gene. SUR1 is encoded by the *ABCC8* gene (ATP-binding cassette transporter sub-family C member 8), and the *ABCC9* gene encodes SUR2A and SUR2B as different splices. Interestingly, $K_{ir}6.1$ and SUR2 are at the same locus (12p12.1 human/6qG2 mouse) and $K_{ir}6.2$ and SUR1 are at the same locus (11p15.1/7qB4). The relationship between these four genes, the proteins produced from the genes, and their chromosomal loci are shown in Figure 2.
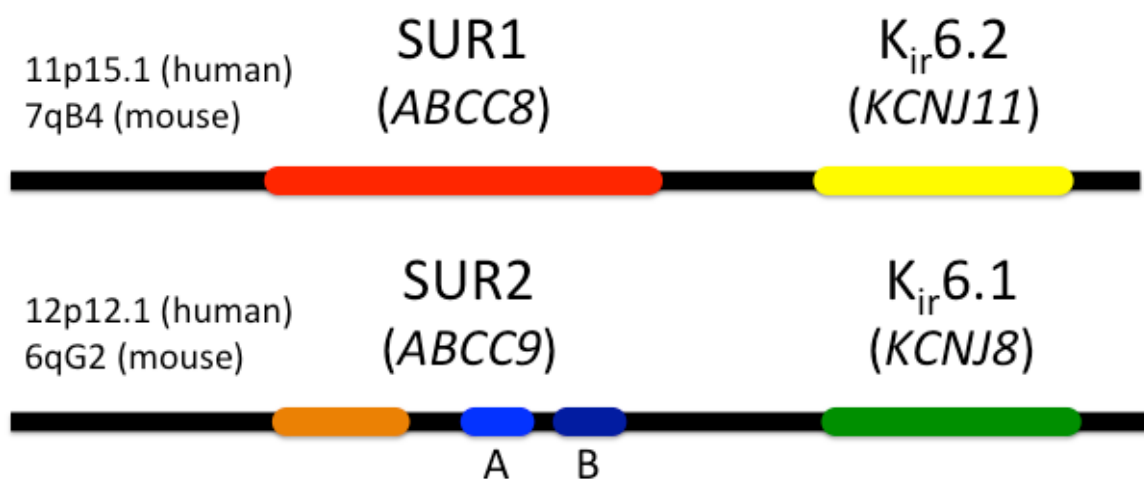
Figure 2.   Chromosomal loci showing SUR1, SUR2A/B, $K_{ir}6.1$, and $K_{ir}6.2$.

In all, there are three SUR and two $K_{ir}6$ proteins, for a total of six possible combinations if only one of each of SUR and $K_{ir}6$ are present in a K_{ATP} channel (as is currently understood):

- SUR1/K_{ir}6.1: Type 1 (sweet) taste (Yee, Sukumaran et al. 2011)
- SUR2B/K_{ir}6.1: Vascular smooth muscle (Seino and Miki 2003); myometrium (Curley, Cairns et al. 2002)
- SUR1/K_{ir}6.2: Pancreatic alpha cells (Gromada, Ma et al. 2004); pancreatic beta cells (Seino, Takahashi et al. 2012)
- SUR2A/K_{ir}6.2: Cardiac muscle and skeletal muscle (Seino and Miki 2003)
- SUR2B/K_{ir}6.2: Non-vascular smooth muscle (Seino and Miki 2003)

However, SUR2A/K_{ir}6.1 has yet to be reported.

K_{ATP} channels are ubiquitous throughout the body. Of interest here is their existence in the plasma membrane (referred to as "K_{ATP}"), but they are reported to exist in both the mitochondria "mitoK_{ATP}" (Garlid and Halestrap 2012) and the nucleus "nucK_{ATP}" (Quesada, Rovira et al. 2002). The roles of K_{ATP} channels are varied but are all related to energy regulation.

- Regulation of smooth muscle tone (Flagg, Enkvetchakul et al. 2010)
- Regulation of insulin secretion (Seino, Takahashi et al. 2012)
- Regulation of glucagon secretion (Gromada, Ma et al. 2004)
- Taste of sweet by the tongue (Yee, Sukumaran et al. 2011)
- Myometrium for increased excitability in late pregnancy (Curley, Cairns et al. 2002)
- Prevention of fiber damage in skeletal muscles from supercontraction (Cifelli, Bourassa et al. 2007)

Of particular interest are the roles in cardiac and skeletal muscle. A complicating factor in teasing apart the role of K_{ATP} channels in these tissues is that they have the same

isoform (SUR2A/K_{ir}6.2). This will be addressed later when discussing the transgenic mouse models.

K_{ir}6.2 knockout mice (K_{ir}6.2-KO) have been created (Miki, Nagashima et al. 1998) and studied. K_{ir}6.2-KO mice reveal numerous different phenotypes:

- Hyperphagia (Alekseev, Reyes et al. 2010; Park, Choi et al. 2011)
- WT-similar blood glucose, triglyceride, and free fatty acid levels (Alekseev, Reyes et al. 2010)
- Increased energy expenditure (Alekseev, Reyes et al. 2010)
- Increased neuropeptide Y (Park, Choi et al. 2011)
- Increased oxygen consumption in hearts (Alekseev, Reyes et al. 2010)
- Diet-induced obesity resistance (Alekseev, Reyes et al. 2010; Park, Choi et al. 2011)
- Sympathetic-induced arrhythmia and sudden death (Zingman, Hodgson et al. 2002)
- Lack of cardiovascular metabolic improvement from exercise (Kane, Behfar et al. 2004)
- Increased skeletal muscle injury from exercise (Kane, Behfar et al. 2004)
- Increased mortality of chronic hyperaldosteronism-caused hypertension (Kane, Behfar et al. 2006)
- Calcium overload, increased QT_c interval, and hypertension-induced congestive heart failure (Kane, Behfar et al. 2006)
- Increased susceptibility of generalized seizures (Yamada, Ji et al. 2001)

This list of phenotypic effects from K_{ir}6.2 knockout mice underscores and underrepresents the breadth of expression and functionality of K_{ATP} channels. Additionally, intact K_{ATP} channels are critical for cardioprotection under ischemic stress (Kane, Liu et al. 2005), a phenomenon that may also involve mitoK_{ATP} channels (Holmuhamedov, Jahangir et al. 2004).

ATP-sensitive potassium channels, as the name implies, are potassium channels that are sensitive to the concentration of ATP. More specifically: the concentration ratio of [ATP]/[ADP]. ATP inhibits $K_{ir}6$ and MgADP binds to SUR to un-inhibit ATP on $K_{ir}6$. Statistically, this leads to closing the $K_{ir}6$ pore with high [ATP]/[ADP] and opening the $K_{ir}6$ pore with low [ATP]/[ADP]. Additionally, it has been reported that K_{ATP} channels are activated by an intracellular pH reduction from 7.19 to 6.45 (Standen, Pettit et al. 1992) and by extracellular adenosine (Barrett-Jolley, Comtois et al. 1996). This makes K_{ATP} channels unique in that their activity is gated by energetic state.

K_{ATP} channels can be controlled pharmacologically through both agonists and antagonists. The SUR subunits respond to sulfonylureas and they act as antagonists to close the channels. Glyburide (USAN)/glibenclamide (INN) is one sulfonylurea commonly used when working with K_{ATP} channels. Pinacidil is one agonist of K_{ATP} channels that functions to open them (often used with 2,4-dinitrophenol (DNP) to reduce [ATP]/[ADP]).

One congenital disease caused by K_{ATP} channels is chronic hyperinsulinism (CHI). In CHI, either SUR1 or $K_{ir}6.2$ carry a reduction- or loss-of-function mutation that leads to pancreatic beta cells that are persistently depolarized and chronically secreting insulin regardless of blood glucose levels (Yan, Lin et al. 2007). Another disease, permanent neonatal diabetes mellitus (PNDM), can arise from mutations in either *KCNJ11* ($K_{ir}6.2$) or *ABCC8* (SUR1) that then lead to a gain in function that presents with chronic hyperpolarization and, thus, less sensitive to rising ATP resulting from hyperglycemia (Rubio-Cabezas, Klupa et al. 2011). Mutations in *ABCC9* (SUR2) have been found to be involved in cardiomyopathy and congestive heart failure (Bienengraeber, Olson et al. 2004; Kane, Liu et al. 2005). K_{ATP} channels have also been implicated in neuroprotective roles and as a possible therapeutic target for reduction of inflammation in multiple sclerosis and other neuroinflammatory diseases (Virgili, Espinosa-Parrilla et al. 2011).

2.3 Potential Measurement

Separation of charges, either electrons or chemical ions, results in a voltage potential between the charges and is rooted in Coulomb's Law. This voltage can be measured directly between the separated charges, or indirectly through the electric fields they produce. When measuring the voltage of a battery, the voltage is measured directly, but when an FM radio measures the voltage from its antenna it is indirectly measuring the electromagnetic field produced by the transmitter antenna. Direct and indirect measurement can be done in biological systems, and each has benefits and limitations.

The electrocardiogram (ECG), electroencephalogram (EEG), and electromyogram (EMG) measure potentials indirectly through the electric fields produced by cardiac muscle cells, cerebral neurons, and skeletal muscle cells, respectively. The EMG can be performed in two different ways. The first is with a needle electrode inserted into the muscle and measures the field in proximity to the needle. The second is through an electrode placed non-invasively on the skin (this method is known as surface EMG or sEMG). To measure the potential of cells, the ions must be measured directly instead of indirectly by the electric fields they produce; therefore, neither is suitable to record the membrane potential or the action potentials of individual myocytes.

In 1883, an electrode was devised (Yang and Kittnar 2010) that used two wires: one placed on intact epicardium and one placed on injured epicardium. The difference between these wires produced a recording of action potentials that had only one polarity and were thus called mono-phasic action potentials (MAP's). The exact biophysical basis of what the MAP electrode measures continues to be debated (Yang and Kittnar 2010). However, the MAP was validated by correlating (r=0.96±0.03) the MAP recordings with intracellular action potential recordings (Franz, Burkhoff et al. 1986) and this permits connecting MAP recordings to morphological changes in action potential changes and thus they have classically been used as an indicator of action potential duration. However, the recorded amplitude depends upon the contact pressure. This limits the

value of the absolute voltages recorded. To record cells with meaningful absolute values, only one method remains: the microelectrode.

2.4 Microelectrode

The microelectrode (ME) is a glass pipette with small tip diameter (<1 μm) that is filled with a salt solution and a metal wire. According to (Halliwell, Whitaker et al. 1987), this type of microelectrode was pioneered by (Ling and Gerard 1949). ME's can be purchased commercially or, more commonly, created with a specialized instrument called a pipette puller. (Pulling pipettes by hand produces pipettes that vary more than those mechanically produced and is not generally recommended.) Pipette pullers create pipettes by applying heat to a small region and then applying a force to pull the tube apart and create two symmetrical pipettes. The pipette is then filled with the desired solution and a wire is inserted into the pipette to make it an electrode.

The ME, unlike EMG and MAP, is used to pierce the plasma membrane of individual cells. This transmembrane approach, in conjunction with a reference electrode outside the cell, is used to directly measure the membrane potential. Each electrode acts as a half-cell to convert an ionic current into an electron current in the metal wire. A specialized amplifier and acquisition systems are used to record from these circuits and are quite common today in electrophysiology labs.

For some cell types, the ME is quite suitable. However, for striated muscle the ME has one significant limitation that makes it unsuitable. The micropipette used to make the ME is made of glass and is particularly fragile. It is particularly problematic that the only remaining technique capable of studying the desired functionality is incompatible with the cell's functionality: movement. One means around this is to uncouple excitation from contraction and eliminating the movement. For example, with 2,3-butanedione monoxime (BDM) (Røed 1993) or blebbistatin (Kovacs, Toth et al. 2004), but this creates a non-physiological testing condition (non-movement) and is undesirable. The problem

presented with the ME and non-stationary cell is that the micropipette tip is rigidly connected to the support that the muscle is contracting against. This creates the relative movement that leads to the ME tip breaking and/or un-impaling with potential of impaling other cells as well.

<div align="center">2.5 Floating Microelectrode</div>

An extension of the ME is the floating microelectrode (FME). The FME uncouples the inertia behind the pipette by cutting the pipette above the shoulder and discarding the shank. This yields a very small pipette (~5 mg) that is suspended by a small (0.005" diameter) electrode wire. The wire is wedged into the tip to keep the tip suspended by the glass-wire friction. Otherwise, FME does not differ technically from the ME. What is different is the cells and data the FME provides access to. The FME permits recording of skeletal muscle *in situ* that is under more physiological conditions than either isolated cell or contraction-uncoupled cells.

Though FME permits recording of cells *in situ*, it is unfortunately not a panacea. The FME can still be subjected to un-impalement from motion, but not as likely as with the ME. The FME is still limited to all of the limitations of transmembrane recording since the FME is fundamentally interacting in the same manner as the ME. For example, both the ME and the FME can only access the top layer (or few layers) of exposed cells.

Since the FME is suspended from a small wire then gravity is a significant determinant of possible approach vectors to the muscle. Good practice with a FME is to use a micromanipulator with one degree of freedom that operates axially along the microelectrode. Combining these means one axis of the manipulator should be vertical along gravity and the FME suspended directly overhead of the cell.

One important limitation of using an *in situ* muscle preparation is that the force measurements of the limb are essentially of no value when comparing effects of superfused drugs. Assuming drug penetration is limited to the top layers of fibers means

that the bulk of fibers are not exposed. This leads to a mixed force recording of treated and untreated fibers with the untreated dominating. For example, the changes in twitch force (Yensen, Matar et al. 2002) in response to a change in superfused potassium concentration would not be measureable. Thus, the force and length recordings are likely only of value as an experimental control.

CHAPTER 3

MATERIALS AND METHODS

3.1 Transgenic Models

Cardiac and skeletal muscle share the same isoform of the K_{ATP} channel: $K_{ir}6.2$ and SUR2A. Two transgenic models based on the FVB/N mouse strain were used to permit tissue specificity of attenuation of K_{ATP} expression in skeletal and cardiac muscle. Both models are established in the literature so they will be discussed only briefly.

Both models utilize $K_{ir}6.1AAA$ in which a Gly-Phe-Gly is replaced in wild type $K_{ir}6.1$ with Ala-Ala-Ala to disrupt pore conduction (Tong, Porter et al. 2006). The chicken β-actin (CX1) promoter is combined with eGFP, a STOP codon, and the $K_{ir}6.1AAA$ to make Tg[CX1-eGFP-$K_{ir}6.1AAA$] mice (Figure 3). A functional portion of the eGFP and associated STOP codon are floxed such that functional eGFP and expression of $K_{ir}6.1AAA$ are mutually exclusive. Cre recombinase ("Cre") is combined with tissue specific promoters to get tissue-specific expression. For cardiac muscle, Cre recombinase is combined with the alpha-myosin heavy chain (αMHC) promoter to make Tg[αMHC-Cre] mice (Figure 4); and for skeletal muscle it is combined with myogenic differentiation 1 (MyoD) promoter to make Tg[MyoD-Cre] mice (Figure 5). This method of tissue-specific expression is known by the Cre-loxP system and has been used quite extensively.

The $K_{ir}6.1AAA$ is dominant negative over both $K_{ir}6.1$ and $K_{ir}6.2$ subunits so any K_{ATP} channel with one or more $K_{ir}6.1AAA$ renders the pore statistically non-functional (Tong, Porter et al. 2006). Expression of $K_{ir}6.1AAA$ is sufficiently high to reduce K_{ATP} current by at least 80-85% (Tong, Porter et al. 2006; Alekseev, Reyes et al. 2010; Zingman, Zhu et al. 2011).
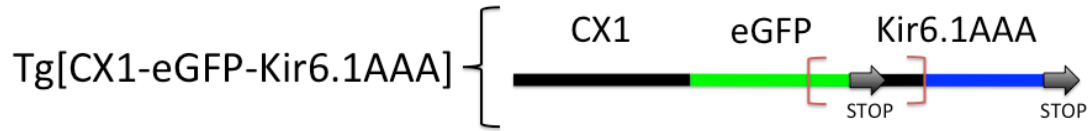
Figure 3.   Transgenic model containing eGFP and $K_{ir}6.1AAA$ (GFP(+) controls). LoxP sites indicated with brackets and floxed region between brackets.
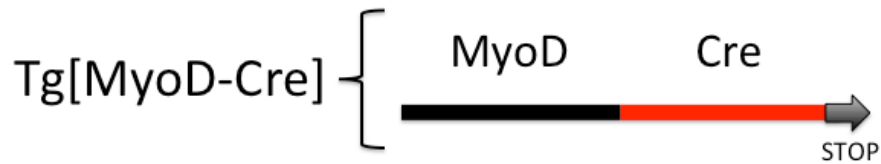
Figure 4.   Transgenic model containing Cre recombinase with the MyoD promoter for skeletal muscle specific expression of Cre recombinase.
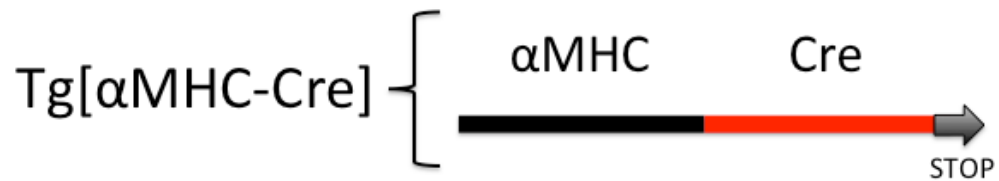
Figure 5.   Transgenic model containing Cre recombinase with the αMHC promoter for cardiac muscle specific expression of Cre recombinase.
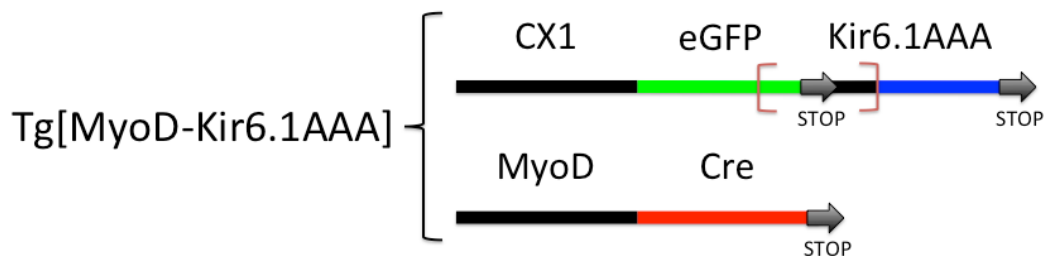
Figure 6.   Transgenic model containing both $K_{ir}6.1AAA$ and MyoD-promoted Cre recombinase.
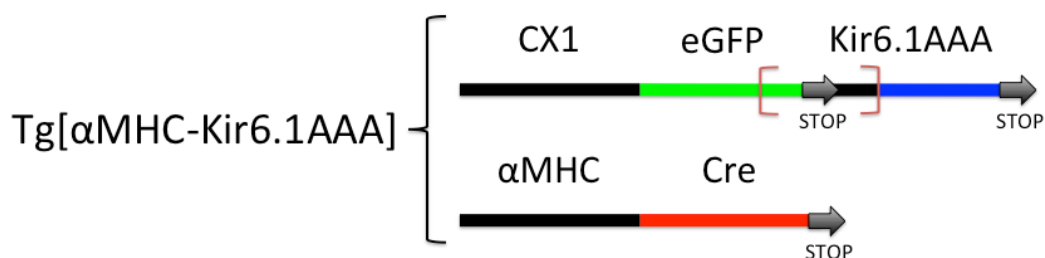
Figure 7.   Transgenic model containing both $K_{ir}6.1AAA$ and αMHC-promoted Cre recombinase.

Tg[CX1-eGFP-$K_{ir}6.1AAA$] mice are bred with Tg[αMHC-Cre] mice to produce Tg[αMHC-$K_{ir}6.1AAA$] mice (Figure 6) for the desired tissue selection of cardiac myocytes with non-functional sarcolemmal K_{ATP} channels. The Tg[CX1-eGFP-$K_{ir}6.1AAA$] mice are GFP(+)/Cre(−) and designated as GFP(+) control mice. The GFP(+)/Cre(−) mice have similar $K_{ir}6.1$ mRNA expression as WT littermates and GFP(+)/Cre(+) lack functional K_{ATP} channels (Malester, Tong et al. 2007). Figure 8

shows what portion of CX1-eGFP-K$_{ir}$6.1AAA that would be transcribed based upon the presence of absence of Cre recombinase.

Similarly, this process was repeated with Tg[MyoD-Cre] that has been shown to cause skeletal muscle specific expression of Cre recombinase (Chen, Mortimer et al. 2005). When bred with Tg[CX1-eGFP-K$_{ir}$6.1AAA] mice they produce Tg[MyoD-K$_{ir}$6.1AAA] mice (Figure 7). The Tg[CX1-eGFP-K$_{ir}$6.1AAA] mice are designated GFP(+) control mice.
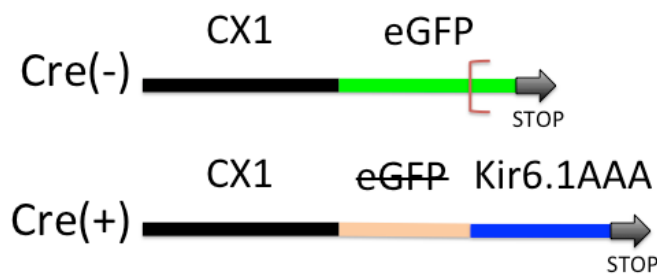
Figure 8.   The resulting portions of CX1-eGFP-K$_{ir}$6.1AAA, as would be transcribed, based upon absence ("Cre(-)") or presence ("Cre(+)") of Cre recombinase due to tissue-specific promoter.

In all, there are five transgenic mice outlined above. The first three are singly transgenic and the last two are doubly transgenic from crossbreeding the first three appropriately.

- Tg[CX1-eGFP-K$_{ir}$6.1AAA]
- Tg[MyoD-Cre]
- Tg[αMHC-Cre]
- Tg[MyoD-K$_{ir}$6.1AAA] = Tg[CX1-eGFP-K$_{ir}$6.1AAA] × Tg[MyoD-Cre]

- $Tg[\alpha MHC-K_{ir}6.1AAA] = Tg[CX1-eGFP-K_{ir}6.1AAA] \times Tg[\alpha MHC-Cre]$

In the entirety of this work, "GFP(+)" denotes $Tg[CX1-eGFP-K_{ir}6.1AAA]$ and "TG" denotes either $Tg[MyoD-K_{ir}6.1AAA]$ or $Tg[\alpha MHC-K_{ir}6.1AAA]$ depending on if the context is skeletal or cardiac muscle, respectively.

These mouse models with significantly reduced expression of function K_{ATP} channels in heart and skeletal muscles are used to determine the effect of K_{ATP} channel function on action potential morphology as a function of metabolic state.

3.2 Monophasic Action Potentials

The MAP electrode (EP Technologies; Sunnyvale, CA) was placed on left ventricular epicardium on hearts that were cannulated through the aorta and retrogradely perfused with Krebs-Henseleit (see Appendix A). A bipolar platinum catheter (NuMed; Hopkinton, NY) was placed in the apex of the right ventricle after mechanically dissociating the AV node. The heart was paced (Bloom Electrophysiology, Fischer Imaging Corp.; Denver, CO) through the platinum catheter. The MAP electrode was amplified (IsoDam; World Precision Instruments; Sarasota, FL) and recorded at 2 kHz (LabView; National Instruments; Austin, TX). Analysis was performed only on those recordings in which the MAP electrode remained stable and pacing was captured for the entirety of the protocol.

Analysis of the action potentials was performed by a set of custom MATLAB (MathWorks; Natick, MA) scripts (see Appendix C). Each action potential for the entire recording was parameterized with the following parameters:

- Baseline membrane potential immediately prior to the action potential
- Start time of the action potential
- End time of the action potential (coincident with start of next AP)
- Total action potential length (end minus start), which equals the pacing cycle length

- Action potential peak amplitude

- Action potential duration at 90% repolarization (APD_{90})

Key parameters — start time, baseline membrane potential, action potential amplitude, and APD_{90} — are shown graphically in Figure 9.
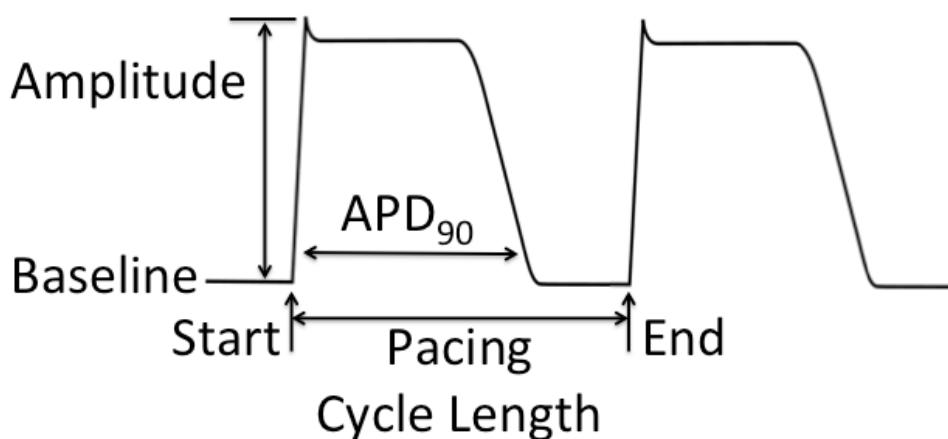
Figure 9.   A model of an action potential showing start time, baseline membrane potential, action potential amplitude, and APD_{90}.

The desired parameter is the APD_{90}, which is the width of the action potential at 90% repolarization. Reduction in the duration of the action potential is known to correlate with reduction in energy expenditure (Zingman, Zhu et al. 2011). So by examining the changes in the MAP APD_{90}, the load on the energetic state can be evaluated.

To compare the APD_{90} between action potentials and between mice, the last action potential of the previous pacing cycle length was taken as the reference. The APD_{90} of each action potential in the subsequent cycle length was subtracted from the reference APD_{90} to yield a time-series of ΔAPD_{90} values.

Two experiments were performed using the MAP electrode. The first experiment paced the heart within its physiological range at cycle lengths of 150, 130, 100, and 80 ms for 3 minutes each for a total of 12 minutes. Figure 10 shows these pacing cycle lengths and their corresponding heart rates ($HR = 60\times1000/CL$) for this protocol. The resulting action potentials recorded with the MAP electrode were analyzed for the above parameters. The ΔAPD_{90} values were compared as described above for the duration of the 12 minutes and grouped by WT, WT with glyburide, and TG mice. Each group was subdivided into mice that were kept under sedentary conditions and mice that were put through an exercise regimen (see Appendix B).
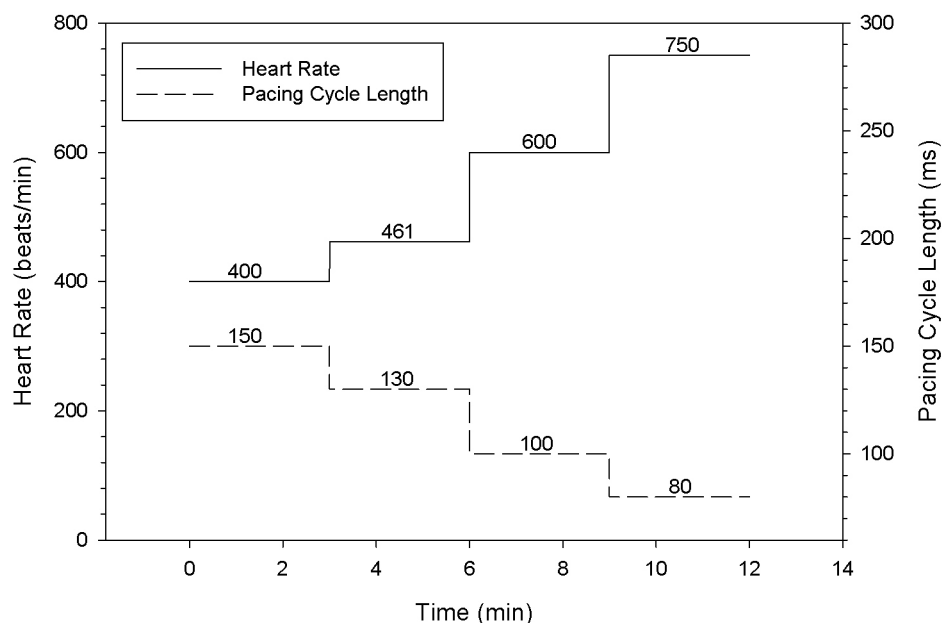
Figure 10. Protocol showing cycle length (dashed) and heart rate (solid) for each step in the protocol.

The second experiment paced the heart constantly at a cycle length of 130 ms and hypoxia was induced by switching from Krebs-Henseleit bubbled with 95% O_2/5% CO_2

to a separate Krebs-Henseleit reservoir bubbled with 95% N_2/5% CO_2. The resulting

action potentials recorded with the MAP electrode were analyzed for the above

parameters. The ΔAPD_{90} values were compared as described above and grouped by WT,

WT with glyburide, GFP, and TG mice.

3.3 Floating Microelectrode

The floating microelectrode (FME) setup consists of a rack of electronics with the

experiment performed inside a Faraday cage on a vibration isolation table. The

electronics setup is shown as a block diagram in Figure 11.
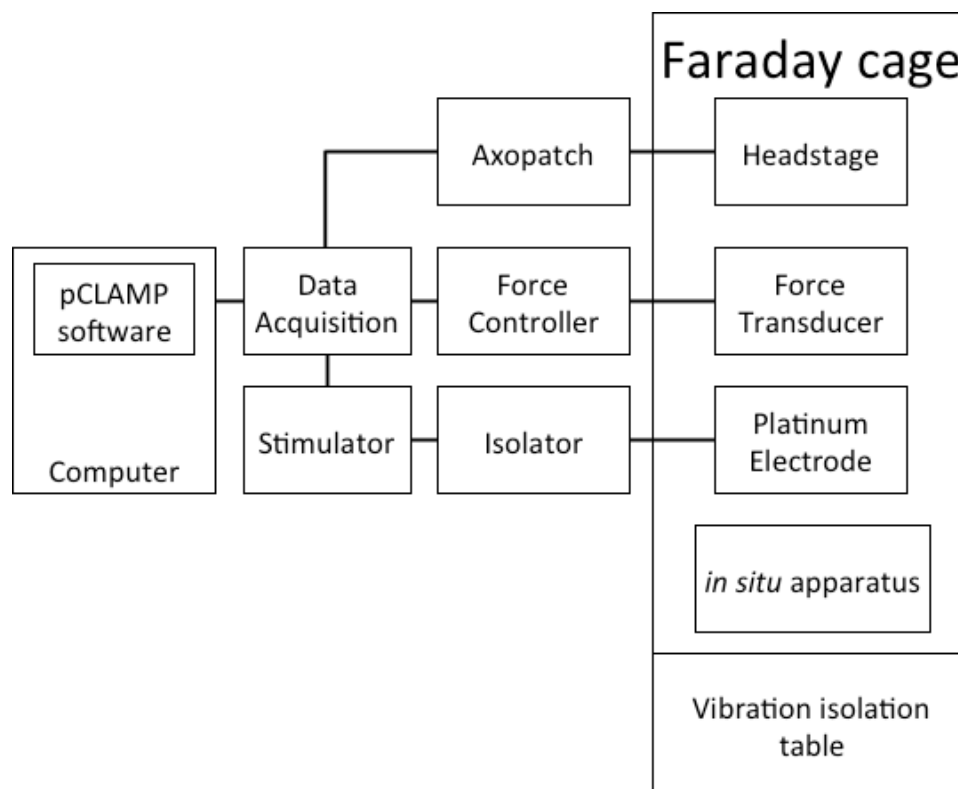
Figure 11. Block diagram of the floating microelectrode electronics setup.

The vibration isolation table (VH3648; Newport; Irvine, CA) has three key components: the base, the tabletop, and the Faraday cage. The base includes the pneumatic control system to dampen vibrations of the tabletop. The Faraday cage (FC3648; Newport; Irvine, CA) is mounted on top of the tabletop and aids in reducing electromagnetic noise. Inside the Faraday cage includes the *in situ* apparatus (809B; Aurora Scientific; Aurora, Ontario, Canada) with force transducer (305C; Aurora Scientific); the amplifier headstage (CV203-BU; Axon Technologies); buffer solution(s); isoflurane vaporizer; and miscellaneous mounting hardware. Under the table is a temperature bath (6200 R20F; Fisher Thermo; Hampton, NH) to control the temperature of the *in situ* apparatus and solutions. Figure 12 shows a cross-sectional cartoon showing the proximal end of the tibialis anterior (TA) secured to the *in situ* apparatus and the distal end secured to the force transducer. (In Figure 12, the rest of the mouse is not drawn for clarity. With the exceptions of removal of the muscle fascia and cutting of the distal tendon, the mouse is left intact.)

The electronics rack contains the computer running pCLAMP (Axon Technologies) that interfaces with the digital acquisition (DAQ) device (Digidata 1440A; Axon Technologies). The DAQ interfaces with the amplifier, the force transducer, and the stimulator and records with a sampling frequency of 25 kHz (period=40 μs).

The amplifier is the same used for patch clamping. The amplifier (Axopatch 200B; Axon Technologies) is in the electronics rack that uses a headstage (CV 203BU; Axon Technologies/Molecular Devices) inside the Faraday cage that connects to the FME through the Ag/AgCl wire (see Appendix D).

The force transducer is mounted to the *in situ* apparatus that the mouse is secured to. The force transducer is mounted via a 3-axis manipulator and is connected to the controller that is outside of the Faraday cage and in the electronics rack. This controller is capable of operating in isometric and isotonic modes.
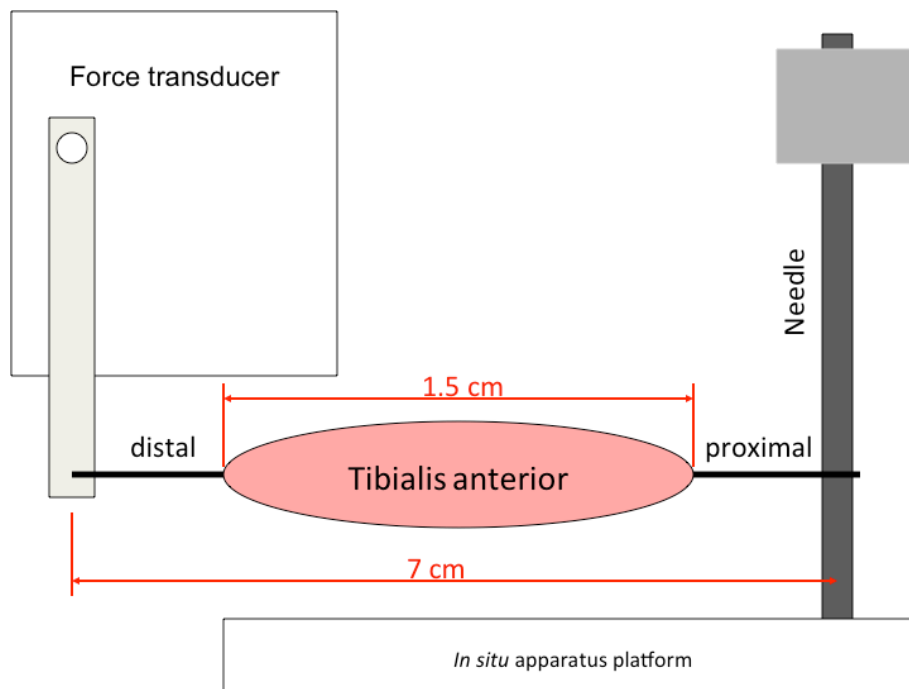
Figure 12. Cross-section view of the tibialis anterior suspended between the force transducer and needle securing the knee. (Remainder of mouse not drawn for clarity.)

Stimulation of the sciatic nerve starts as a digital pulse in pCLAMP and is converted to an analog signal with desired waveform of pulse width of 500 µs by a stimulator (Accupulser A310; World Precision Instruments; Sarasota, FL). The stimulus is then routed through a stimulus isolation unit (A365 SIU; World Precision Instruments) to electrically isolate the stimulus to reduce the noise recorded by the amplifier. The stimulus is delivered to the sciatic through a custom-made platinum electrode.

Initial anesthesia is induced with intraperitoneal avertin (see Appendix A) and maintained with inhaled isoflurane at approximately 50 breaths per minute (~1.0-1.5% v/v).

Pipettes for the FME were pulled on a horizontal puller (P-1000; Sutter Instrument; Novato, CA) with borosilicate pipettes (1B150F; World Precision Instruments). Each pipette was filled with 3 mol/L potassium chloride (3M KCl) because

the dominant intracellular cation is potassium. A 0.005" silver wire coated with polytetrafluoroethylene (PTFE; "Teflon") was mechanically stripped at both ends and electrochemically plated with silver chloride on one end (see Appendix D) to produce a Ag/AgCl electrode. The wire was coiled around a cylinder (~1 cm diameter) by one turn to produce a spring-like shape in the middle. The micropipette was scored with a carbide utility blade a couple of millimeters above the shoulder and gently snapped between fingers. The shank was discarded. The silver chlorided end of the wire was inserted into the tip sufficiently to create enough friction to support the weight of the tip (~5 mg) and the non-silver chlorided end was attached to the headstage.

Each experimental trial is performed with a new FME tip and every tip is zero-adjusted in a pool of Tyrode's solution (see Appendix A) with the reference electrode. Zero adjustment was done in the membrane test tool of pCLAMP and the pipette resistance was simultaneously measured and recorded.

The tibialis anterior (TA) muscle was exposed through gross dissection of the skin and muscle fascia. The proximal end was secured to the *in situ* apparatus with a 30G 1-1/2" needle through the patellar tendon at the knee; the distal tendon was tied with 3/0 silk and looped through the lever arm of the force transducer. The TA was continuously superfused with Tyrode's solution. Alternatively, as protocol required, additional Tyrode's solutions containing 10 μM glyburide, 100 μM pinacidil, or glyburide plus pinacidil were used.

The temperature of the *in situ* platform and superfusion solutions were maintained by a temperature bath at 34.8°C. Solutions were pre-warmed by jacketed columns and fed into a multi-input manifold, then re-warmed immediately before dripping by a jacketed spiral tube, which yielded a temperature of Tyrode's solution at the TA of approximately 32°C.

Each mouse was anesthetized, dissected to expose the TA, secured to the *in situ* apparatus, and aesthesia plane maintained under isoflurane. The muscle was secured to

the force transducer and platinum electrode was introduced in proximity to the sciatic

nerve. The muscle was placed through the desired protocol (see Appendix B).

CHAPTER 4

RESULTS

4.1 K_{ATP} channels promote APD_{90} shortening of cardiac

action potentials in exercised mice

K_{ATP} channels have been shown to shorten the APD_{90} through increases in heart rate (Alekseev, Reyes et al. 2010). Increasing the heart rate imposes a higher workload upon the heart and the changes in APD_{90} resulted from the level of K_{ATP} expression in WT, WT with glyburide, and $K_{ir}6.2$-KO. To further understand the relationship between K_{ATP} channels and changes in APD_{90}, the transient response was analyzed in various mouse models with varying expression of functional K_{ATP} channels. Exercised WT had a 50% increase in both functional K_{ATP} channels and K_{ATP} current, while TG had an 80-85% reduction (Zingman, Zhu et al. 2011). Glyburide is a potent blocker of K_{ATP} channels and exercise did not increase functional K_{ATP} channels in TG mice, likely due to dominant negative effect of the $K_{ir}6.1AAA$ mutant gene (Zingman, Zhu et al. 2011).

Monophasic action potentials were recorded and analyzed for the APD_{90} change relative to a step change in heart rate (ΔAPD_{90}) and shown in Figure 13. Action potential durations showed a rapid drop, a rapid rebound toward baseline, and then an overdamped response to the steady state. Exposure to exercise had no discernable effect on both WT with glyburide and TG mice for all pacing transitions. For WT mice, exercise had a significant effect on magnitude of action potential duration shortening for the 130-to-100 transition and a partial significant effect on APD_{90} shortening for the 100-to-80 transition. There are two effects on the transitions for exercised WT mice.

The first is that APD_{90} shortening occurred more quickly. To quantify this, the delay time (or half time) was calculated. The delay time ($t_{1/2}$) is defined as the time for the response to reach halfway between maximum and steady state and is shown in Figure

15. Exercised WT mice showed significant reduction in the delay time as compared to all other groups in the 130-to-100 and 100-to-80 transitions, but there was no significant difference for the 150-to-130 transition (Figure 15). Similarly, sedentary WT mice were significantly reduced as compared to all other groups except exercised WT.
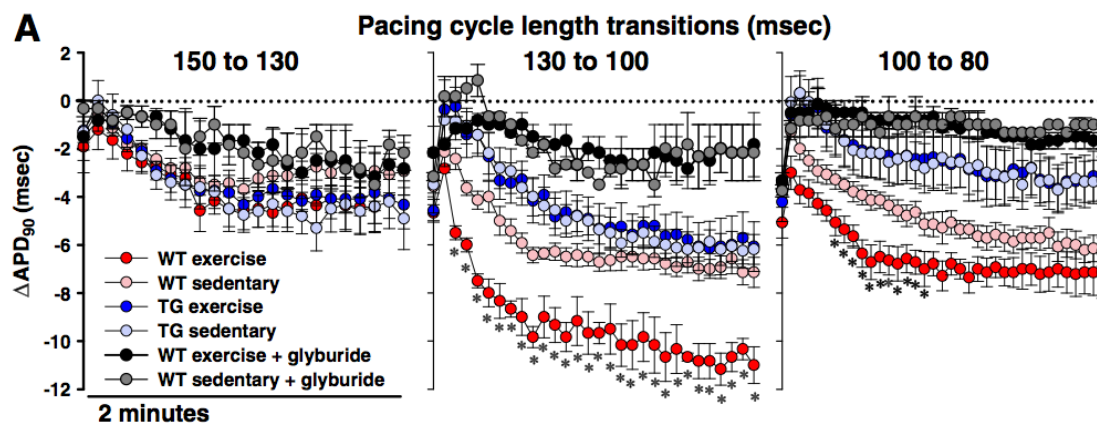
Figure 13. The three transitions showing ΔAPD_{90} relative to the last AP from previous cycle. (Adapted from (Zingman, Zhu et al. 2011).)
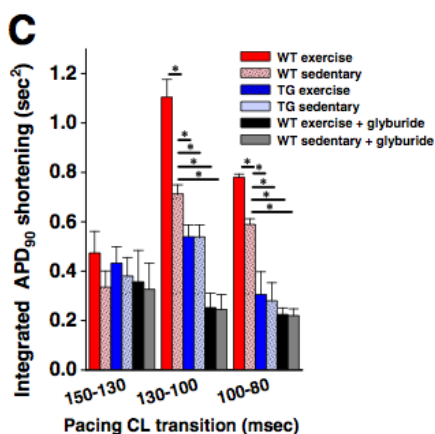
Figure 14. Area under the curve (AUC) calculations for all three transitions after each change in pacing cycle length. From left to right in each group: WT exercise, WT sedentary, TG exercise, TG sedentary, WT with glyburide exercise, and WT with glyburide sedentary. (Adapted from (Zingman, Zhu et al. 2011).)
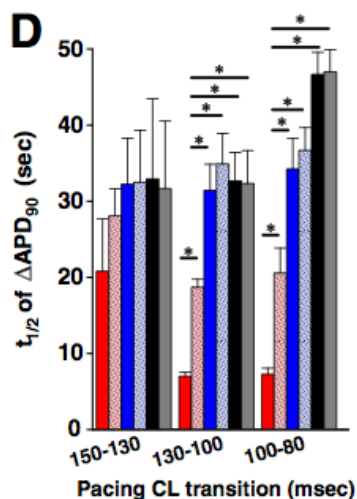
Figure 15. Delay time for all three transitions after each change in pacing cycle length. From left to right in each group: WT exercise, WT sedentary, TG exercise, TG sedentary, WT with glyburide exercise, and WT with glyburide sedentary. (Adapted from (Zingman, Zhu et al. 2011).)

The second is that the amount of shortening is greater. This was quantified by calculating the area under the curve (AUC) and is shown in Figure 14. Larger AUC's incorporate both faster reduction and degree of reduction. Analogous to delay time, exercised WT mice showed a significantly larger AUC than all other groups for the 130-to-100 and 100-to-80 transitions, and sedentary WT mice as well as compared to all other groups except exercised WT.

The lab produced other supporting evidence for the involvement of K_{ATP} channels in the action potential adjustment to changes in workload (i.e., energetic load) (Zingman, Zhu et al. 2011), including:

- Patch clamp of isolated cardiomyocytes showing increased number of K_{ATP} channels in exercised mice (8.59±1.07 vs. 4.66±0.41 channels)
- Increased K_{ATP} current in exercised mice (25.19±2.09 vs.17.75±1.34 pA/pF)

- No difference in number of channels nor in K_{ATP} current for exercise in TG mice (0.94±0.18 vs. 1.1±0.23 channels; 2.3±0.5 vs. 2.5±0.6 pA/pF)

- Increased oxygen consumption with decreased pacing cycle length (i.e., increased heart rate) that was attenuated for hearts with increased functional K_{ATP} channels (i.e., such hearts were more energy efficient)

- Increased SUR2A transcription in exercise (~1.5x vs. sedentary as 1.0)

4.2 Absence of cardiac K_{ATP} channels dampens hypoxic response

The role of K_{ATP} channels in cardiac stress is well known. Since the heart relies on aerobic metabolism, one form of stress is reduction, or elimination, of oxygen as is the case of a myocardial infarction. Monophasic action potentials of isolated hearts with varying number of functional K_{ATP} channels (Zhu, Burnett et al. 2011) were recorded prior to and during hypoxia and analyzed for the APD_{90}. The APD_{90} prior to hypoxia was taken as the reference APD_{90} and ΔAPD_{90} values were calculated from this reference and grouped by WT, WT with glyburide, GFP(+), and TG and is shown in Figure 16.

Action potentials showed an increase in duration almost immediately at the start of hypoxia. All but WT with glyburide then show a decrease toward a steady-state APD_{90}. Both WT and GFP(+) mice show a similar response and reach steady state more quickly than TG mice. From the maximum, the response can be considered an overdamped transient response. One relevant parameter of such transient responses is the delay time. An increase in this parameter is an increase in the dampening.

Delay times were calculated and shown in Figure 17. The difference in delay time between WT and GFP(+) is not significant (45.5±6.3 vs. 38.8±3.6), but TG is significantly longer (60.9±4.7).

The lab also produced supporting evidence for the involvement of K_{ATP} channels in response to hypoxia (Zhu, Burnett et al. 2011), including:

- Patch clamp of isolated cardiomyocytes showing decrease of ~85% in K_{ATP} channel current in the TG model compared to WT and GFP (WT 18.1±2.3, GFP 17.4±1.7, TG 2.5±0.6 pA/pF)
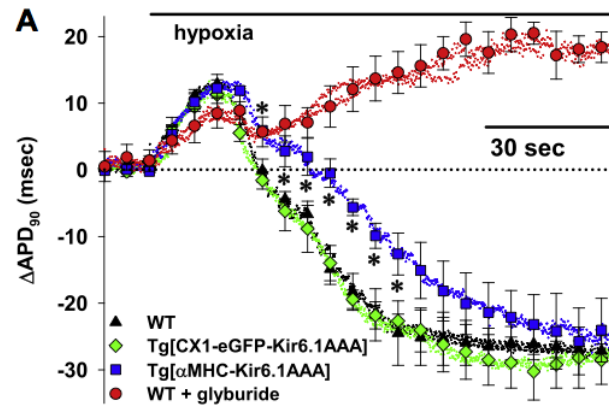
Figure 16. Change in APD_{90} from baseline taken from before start of hypoxia. (Adapted from (Zhu, Burnett et al. 2011).)
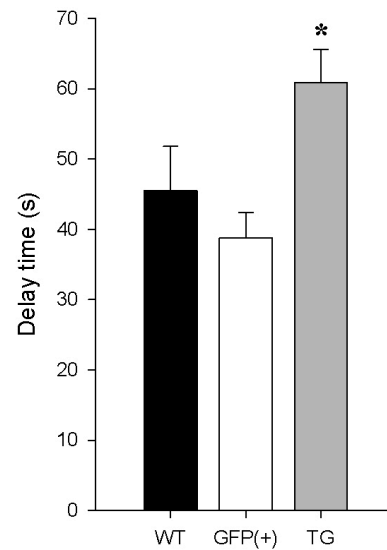
Figure 17. Delay time for each group after inducing hypoxia. (Adapted from (Zhu, Burnett et al. 2011).)

<u>4.3 Membrane potential in murine skeletal muscle follows</u>

<u>a normal distribution</u>

Many random variables of natural and biological origin follow a normal distribution. As a result of many stochastic processes, the membrane potential can be approximated by a normal distribution. Figure 18 shows a histogram of 275 independent membrane potential measurements across WT, GFP(+), and TG mice. The range was [−99.5, −72.0] with mean −83.5, median −83.0, mode −83.0, standard deviation 3.8, skewness −0.78, and kurtosis of 2.2. In comparison, a normal distribution would have a skewness of zero and kurtosis of 3 (or, identically, an excess kurtosis of zero).

In collecting action potentials, those action potentials with membrane potential more positive than −70 mV and negative overshoot were excluded and could account for some of the negative skewness.
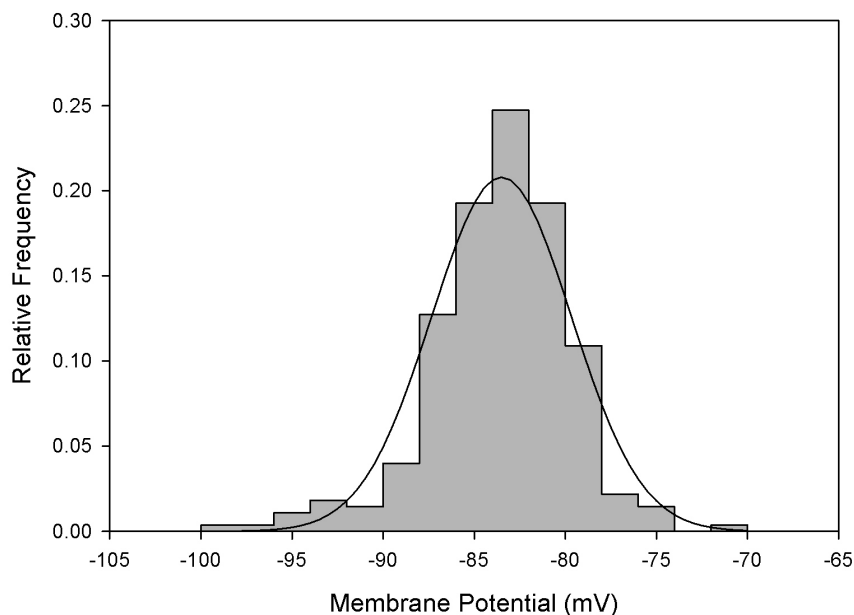
Figure 18. Histogram showing membrane potential across WT, GFP(+), and TG mice, and a Normal(μ=83.5, σ=3.8) distribution is overlaid on the histogram. (N=275)

<u>4.4 Overall statistics of skeletal muscle action potentials</u>

The action potential amplitude and overshoot do not appear to be as normally distributed as the membrane potential. Histograms from WT and GFP(+) mice were created and shown in Figure 19 and Figure 20. The action potential amplitude had a range of [79.3, 140] mV with mean 103.2, median 99.8, mode 98.3, standard deviation 13.3, skewness 0.53, and kurtosis −0.44. The overshoot had a range of [−3, 140] mV with mean 19.7, median 16.4, mode 0, standard deviation 13.8, skewness 0.57, and kurtosis −0.53.

Action potential amplitude and overshoot appear to be heavily influenced by the zero overshoot threshold as indicated by the strong positive skew. Unlike membrane potential where WT, GFP(+), and TG were not different, action potential amplitude and overshoot were different from TG mice and therefore only 210 recordings were analyzed.
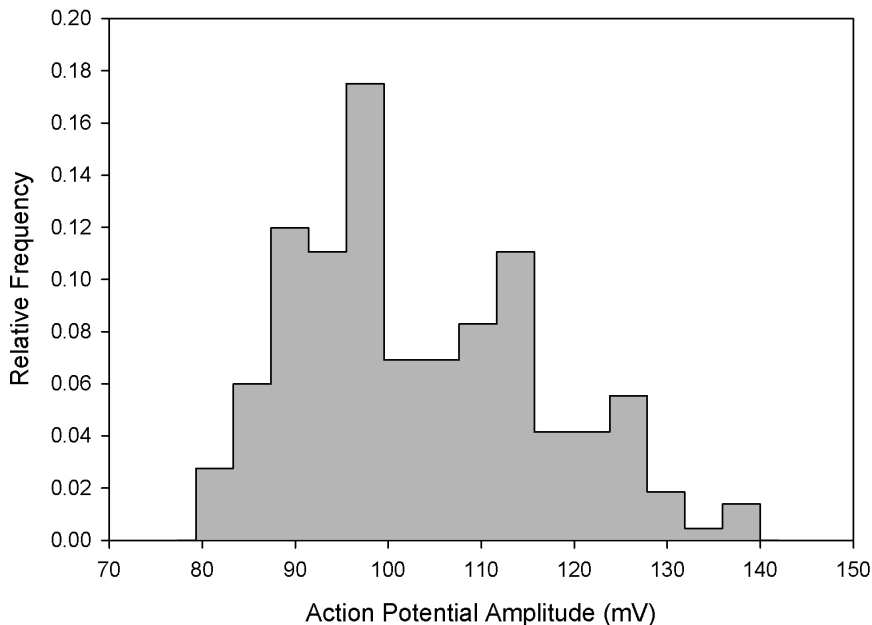
Figure 19. Histogram showing action potential amplitude across WT and GFP(+) mice. (N=210)
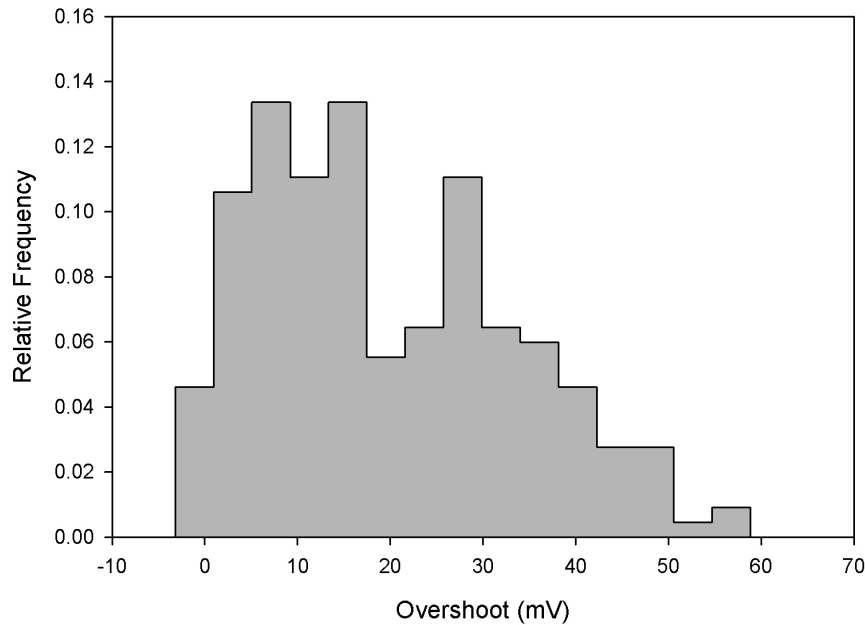
Figure 20. Histogram showing overshoot across WT and GFP(+) mice. (N=210)

4.5 K$_{ATP}$ channels hyperpolarize the membrane under
physiological twitching

The opening of a potassium channel at normal membrane potentials has been known to cause a stabilization of the membrane and reduction in excitability through hyperpolarization. To confirm this experimentally *in situ* with regard to K$_{ATP}$ channels, the floating microelectrode was used on tibialis anterior (TA) muscles. A very low level of workload was applied to the muscle of WT, GFP(+), and TG mice to induce change in energetic state that might affect K$_{ATP}$ channel opening (see Appendix B). In TG skeletal myocytes, it has been shown that there is no measurable K$_{ATP}$ channel current (Alekseev, Reyes et al. 2010).

Various exclusion criteria were applied to identify acceptable action potentials for analysis. The membrane potential had to be more negative than -70 mV. The action potential amplitude had no exclusion criteria. The action potential overshoot for the baseline was chosen to be 15 mV (corresponding to that found in (Gong, Legault et al.

2003)). The overshoot for the twitched step had to be greater than −5 mV because the overshoot was reduced by about 20 mV after twitching. The overshoot for the twitched with glyburide step had to be greater than 7.5 mV because the overshoot increased by 10 mV with glyburide and about 15 mV with pinacidil (see next section).

The membrane potentials were averaged over each group (WT, GFP(+), and TG) and each step of the protocol (baseline, twitched, and glyburide) and shown in Figure 21. The baseline data were not significantly different between mouse groups (p=0.49) or pair-wise between groups (WT vs. GFP: p=0.85; WT vs. TG: p=0.36; GFP vs. TG: p=0.11). WT and GFP(+) showed a significant hyperpolarization after twitching (WT: −82.23±0.42 vs. −87.38±0.93, p=0.0000023; GFP: −82.12±0.29 vs. −82.12±0.29 vs. −88.46±0.95, p=0.0000020) but TG was not significantly hyperpolarized (−82.74±0.25 vs. −83.85±1.19, p=0.35). The twitched data were significantly different between mouse groups (p=0.011); WT and GFP were not significantly different from each other (p=0.42) but WT and GFP were each significantly different from TG (WT vs. TG: p=0.022; GFP vs. TG: p=0.0040). After application of glyburide, all three groups depolarized but only WT and GFP(+) were significantly depolarized (WT: −82.40±1.10, p=0.0015; GFP: −81.36, p=0.00013; TG: −82.13±1.49, p=0.47). The glyburide data were not significantly different between mouse groups (p=0.80) or pair-wise between groups (WT vs. GFP: p=0.51; WT vs. TG: p=0.90; GFP vs. TG: p=0.66).

The action potential amplitudes were averaged over each group and each step of the protocol and shown in Figure 22. The baseline data were not significantly different between mouse groups (p=0.36) or pair-wise between groups (WT vs. GFP: p=0.24; WT vs. TG: p=0.84; GFP vs. TG: p=0.21). All three groups showed a significant reduction after twitching (WT: 111.07±1.10 vs. 97.50±1.36, $p=10^{-12}$; GFP: 113.35±1.64 vs. 100.32±1.42, $p=10^{-8}$; TG: 110.73±1.27 vs. 93.06±1.59, $p=10^{-13}$). The twitched data were significantly different between groups (p=0.0061); WT and GFP were not significantly different from each other but WT and GFP were each significantly different from TG

(WT vs. GFP: p=0.16; WT vs. TG: p=0.042; GFP vs. TG: p=0.0018). After application of glyburide, all three groups increased but only WT was significantly increased (WT: 102.36±2.00, p=0.045; GFP: 102.26±1.91, p=0.49; TG: 98.64±1.68, p=0.075). The glyburide data were not significantly different between mouse groups (p=0.53) or pair-wise between groups (WT vs. GFP: p=0.97; WT vs. TG: p=0.31; GFP vs. TG: p=0.23).

The action potential overshoots were averaged over each group and step of the protocol and shown in Figure 23. The overshoot is a summation of membrane potential and action potential amplitude and can reflect trends seen in either. The baseline data wre not significantly different between mouse groups (p=0.22) or pair-wise between groups (WT vs. GFP: p=0.19; WT vs. TG: p=0.60; GFP vs. TG: p=0.12). All three groups showed a significant reduction after twitching (WT: 28.85±1.01 vs. 10.13±1.25, p=10^{-23}; GFP: 31.23±1.61 vs. 11.86±1.11, p=10^{-18}; TG: 27.99±1.27 vs. 9.21±1.44, p=10^{-16}). The twitched data were not significantly different between groups (p=0.33) or pair-wise between groups (WT vs. GFP: p=0.30; WT vs. TG: p=0.64; GFP vs. TG: p=0.16). After application of glyburide, all three groups significantly increased (WT: 19.96±1.43, p=0.0000041; GFP: 20.89±1.88, p=0.00012; TG: 16.51±1.82, p=0.013). The glyburide data were not significantly different between mouse groups (p=0.34) pair-wise between groups (WT vs. GFP: p=0.69; WT vs. TG: p=0.21; GFP vs. TG: p=0.15).

Table 1 shows two-sided, unpaired t-tests between groups for membrane potential; Table 2 for action potential amplitudes; and Table 3 for overshoot. Additionally, Table 4 shows the number of action potentials for each group of mice for each step of the protocol and Table 5 summarizes the above data from Figure 21, Figure 22, and Figure 23. Table 6 shows the one-way ANOVA p-values between the WT, GFP, and TG groups for each step of the protocol — baseline, twitched, and with glyburide — and for each parameter measured. Table 7 shows the one-way ANOVA p-values between the steps of the protocol for each mouse group and parameter measured. For completeness, Table 8 shows the unpaired, two-sided t-tests between pair-wise groups.

Lastly, Figure 24 shows sample action potentials recorded for each group of mice for each step of the protocol.
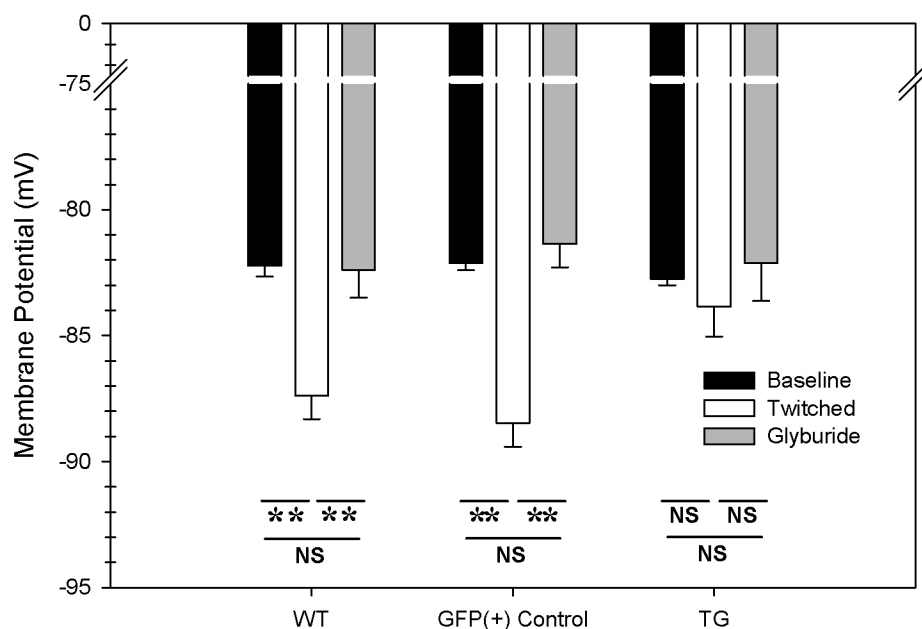
Figure 21. Membrane potential between WT, GFP(+), and TG groups for each step of the glyburide protocol. (*p<0.05; **p<0.01)

Table 1. Two-sided, unpaired t-test values over membrane potential for glyburide data shown in Figure 21. (*p<0.05; **p<0.01)

	Baseline/Twitched	Baseline/Glyburide	Twitched/Glyburide
WT	0.0000023 (**)	0.87	0.0015 (**)
GFP	0.0000020 (**)	0.35	0.00013 (**)
TG	0.35	0.52	0.47
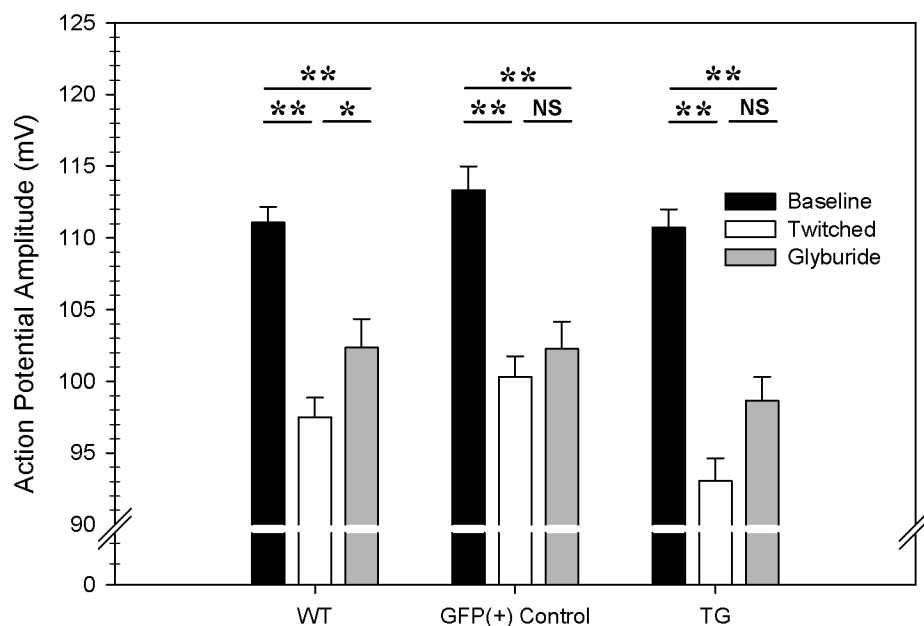
Figure 22. Action potential amplitude between WT, GFP(+), and TG groups for each step of the glyburide protocol. (*p<0.05; **p< 0.01)

Table 2. Two-sided, unpaired t-test values over action potential amplitudes for glyburide data shown in Figure 22. (*p<0.05; **p<0.01)

	Baseline/Twitched	Baseline/Glyburide	Twitched/Glyburide
WT	10^{-12} (**)	0.000075 (**)	0.045 (*)
GFP	10^{-8} (**)	0.000087 (**)	0.49
TG	10^{-13} (**)	0.000017 (**)	0.075
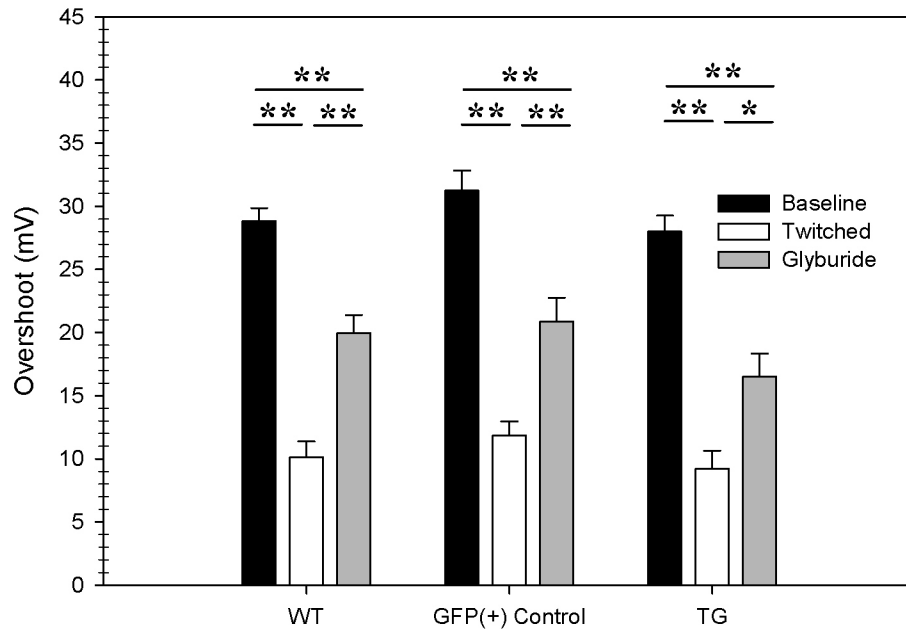
Figure 23. Overshoot between WT, GFP(+), and TG groups for each step of the
glyburide protocol. (*p<0.05; **p<0.01)

Table 3.   Two-sided, unpaired t-test values over overshoot for glyburide data shown in
Figure 23. (*p<0.05; **p<0.01)

	Baseline/Twitched	Baseline/Glyburide	Twitched/Glyburide
WT	10^{-22} (**)	0.0000015 (**)	0.0000041 (**)
GFP	10^{-18} (**)	0.00018 (**)	0.00012 (**)
TG	10^{-16} (**)	0.000048 (**)	0.013 (*)

Table 4.   Number of action potentials for WT, GFP(+), and TG groups and for each step of the glyburide protocol including row and column totals.

	Baseline	Twitched	Glyburide	Totals
WT (N=19)	73	77	40	190
GFP (N=18)	50	87	27	164
TG (N=14)	50	46	14	110
Totals	173	210	81	464

Table 5.   Summary of membrane potential (V_m), action potential amplitude (AP), and overshoot (V_o) as graphed in Figure 21, Figure 22, and Figure 23. (mean±SE)

		WT	GFP(+)	TG
Baseline	V_m	−82.23±0.42	−82.12±0.29	−82.74±0.25
	AP	111.07±1.10	113.35±1.64	110.73±1.27
	V_o	28.85±1.01	31.23±1.61	27.99±1.27
Twitched	V_m	−87.38±0.93	−88.46±0.95	−83.85±1.19
	AP	97.50±1.36	100.32±1.42	93.06±1.59
	V_o	10.13±1.25	11.86±1.11	9.21±1.44
Glyburide	V_m	−82.40±1.10	−81.36±0.92	−82.13±1.49
	AP	102.36±2.00	102.26±1.91	98.64±1.68
	V_o	19.96±1.43	20.89±1.88	16.51±1.82

Table 6.   One-way ANOVA over WT/GFP/TG for each step of the glyburide protocol (baseline, twitched, glyburide) for each parameter (V_m, AP, V_o). (*$p<0.05$; **$p<0.01$)

	V_m	AP	V_o
Baseline	0.48	0.36	0.22
Twitched	0.012 (*)	0.0061 (**)	0.33
Glyburide	0.80	0.53	0.34

Table 7. One-way ANOVA over baseline/twitched/glyburide for mouse group (WT, GFP, TG) for each parameter (V_m, AP, V_o) of the glyburide protocol. (*$p<0.05$; **$p<0.01$)

	V_m	AP	V_o
WT	10^{-6} (**)	10^{-11} (**)	≈ 0 (**)
GFP	10^{-8} (**)	10^{-8} (**)	≈ 0 (**)
TG	10^{-8} (**)	10^{-7} (**)	≈ 0 (**)
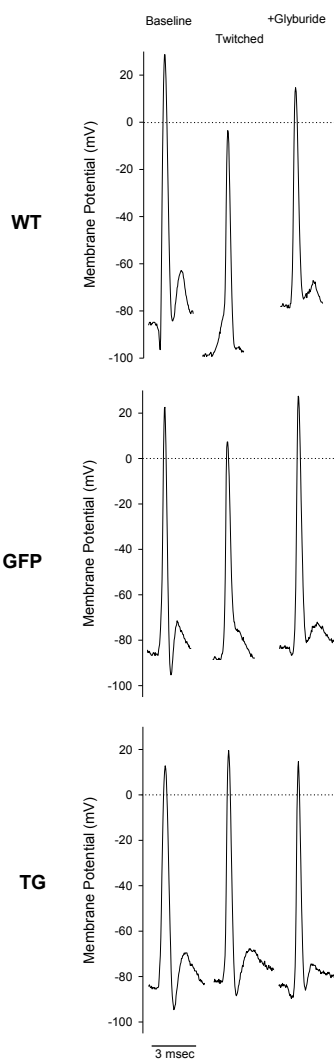
Figure 24. Sample action potentials of the three mouse groups (WT, GFP(+), and TG) and for each step of the glyburide protocol (baseline, twitched, and glyburide).

Table 8. Two-sided, unpaired t-test values pair-wise between groups for each step of the glyburide protocol and parameter measured. (*p<0.05; **p<0.01)

		V_m	AP	V_o
Baseline	WT vs. GFP	0.85	0.24	0.19
	WT vs. TG	0.36	0.84	0.60
	GFP vs. TG	0.11	0.21	0.12
Twitched	WT vs. GFP	0.42	0.16	0.30
	WT vs. TG	0.022 (*)	0.042 (*)	0.64
	GFP vs. TG	0.0040 (**)	0.0018 (**)	0.16
Glyburide	WT vs. GFP	0.51	0.97	0.70
	WT vs. TG	0.90	0.31	0.21
	GFP vs. TG	0.66	0.23	0.15

4.6 K_{ATP} channels hyperpolarize the membrane under pinacidil

In parallel to using physiological twitching with glyburide, experiments were performed without a twitching protocol but with the K_{ATP} channel opener, pinacidil, to WT, GFP(+), and TG mice (see Appendix B).

The action potential exclusion criteria previously established for the twitching and glyburide data were reused for the following data. Briefly, membrane potentials had to be more negative than −70 mV, and the action potential overshoot had to exceed 15 mV, −5 mV, and 7.5 mV for the baseline, pinacidil, and pinacidil with glyburide protocol steps, respectively. Action potentials not meeting these thresholds were excluded from analysis.

The membrane potentials were averaged over each group (WT, GFP(+), and TG) and each of the protocol (baseline, pinacidil, and pinacidil plus glyburide) and shown in Figure 25. The baseline data were not significantly different between mouse groups (p=0.48) or pair-wise between groups (WT vs. GFP: p=0.85; WT vs. TG: p=0.36; GFP

vs. TG: p=0.11). WT and GFP(+) showed a significant hyperpolarization after pinacidil (WT: −82.23±0.42 vs. −90.48±1.60, p=10^{-11}; GFP: −82.12±0.29 vs. −94.17±1.15, p=10^{-21}) but TG was not significantly hyperpolarized (−82.74±0.25 vs. −84.90±0.41, p=0.000018). The pinacidil data were significantly different between mouse groups (p=10^{-5}); only GFP and TG were significantly different from each other but WT and GFP were almost significant (WT vs. GFP: p=0.085; WT vs. TG: p=0.76; GFP vs. TG: p=10^{-9}). After application of pinacidil plus glyburide, all three groups depolarized but only WT and GFP were significantly depolarized (WT: −86.19±1.50, p=10^{-8}; GFP: −84.23±1.13, p=10^{-7}; TG: −81.17±0.78, p=0.61). The pinacidil plus glyburide data were not significantly different between mouse groups (p=0.33) pair-wise between groups (WT vs. GFP: p=0.30; WT vs. TG: p=0.99; GFP vs. TG: p=0.38).

The action potential amplitudes were averaged over each group and each step of the protocol and shown in Figure 26. The baseline data were not significantly different between mouse groups (p=0.36) or pair-wise between groups (WT vs. GFP: p=0.24; WT vs. TG: p=0.84; GFP vs. TG: p=0.21). All three groups showed a significant reduction after pinacidil (WT: 111.07±1.10 vs. 99.98±2.16, p=0.0000033; GFP: 113.35±1.64 vs. 105.32±2.44, p=0.0086; TG: 110.73±1.27 vs. 94.64±1.46, p=10^{-11}). The pinacidil data were significantly different between groups (p=0.0039); only GFP and TG were significantly different from each other (WT vs. GFP: p=0.11; WT vs. TG: p=0.46; GFP vs. TG: p=0.00056). After application of pinacidil plus glyburide, WT and GFP significantly increased and TG decreased (WT: 115.85± 3.47, p=0.00023; GFP: 116.71±3.01, p=0.0068; TG: 93.17±1.04, p=0.73). The pinacidil plus glyburide data were significantly different between mouse groups (p=0.048); GFP and TG were significantly different (WT vs. GFP: p=0.86; WT vs. TG: p=0.26; GFP vs. TG: p=0.016).

The action potential overshoots were averaged over each group and step of the protocol and shown in Figure 27. The overshoot is a summation of membrane potential and action potential amplitude and can reflect trends seen in either. The baseline data

were not significantly different between mouse groups (p=0.22) or pair-wise between groups (WT vs. GFP: p=0.19; WT vs. TG: p=0.60; GFP vs. TG: p=0.12). All three groups showed a significant reduction after pinacidil (WT: 28.85±1.01 vs. 9.49±1.65, p=10^{-16}; GFP: 31.23±1.61, p=10^{-9}; TG: 27.99±1.27 vs. 9.74±1.50, p=10^{-9}). The pinacidil data were not significantly different between groups (p=0.81) or pair-wise between groups (WT vs. GFP: p=0.58; WT vs. TG: p=0.87; GFP vs. TG: p=0.64). After application of pinacidil plus glyburide, WT and GFP significantly increased and TG increased (WT: 29.66±2.88, p=10^{-8}; GFP: 32.48±2.67, p=10^{-7}; TG: 12.00±0.69, p=0.61). The pinacidil plus glyburide data were significantly different between mouse groups (p=0.047); GFP and TG were significantly different (WT vs. GFP: p=0.49; WT vs. TG: p=0.033; GFP vs. TG: p=0.018).

Table 9 shows two-sided, unpaired t-tests between groups for membrane potential; Table 10 for action potential amplitudes; and Table 11 for overshoot. Additionally, Table 12 shows the number of action potentials for each group of mice for each step of the protocol and Table 13 summarizes the above data from Figure 25, Figure 26, and Figure 27. Table 14 shows the one-way ANOVA p-values between the WT, GFP, and TG groups for each step of the protocol — baseline, pinacidil, and pinacidil plus glyburide — and for each parameter measured (membrane potential, V_m; action potential amplitude, AP; and overshoot, V_o). Table 15 shows the one-way ANOVA p-values between the steps of the protocol for each mouse group and parameter measured (some of the p-values calculated are beneath Microsoft Excel's numerical precision and are shown as ≈0). For completeness, Table 16 shows the unpaired, two-sided t-tests between pair-wise groups. Lastly, action potentials recorded for each group of mice for each step of the protocol were sufficiently like those shown in Figure 24 that a figure was not created for this protocol.
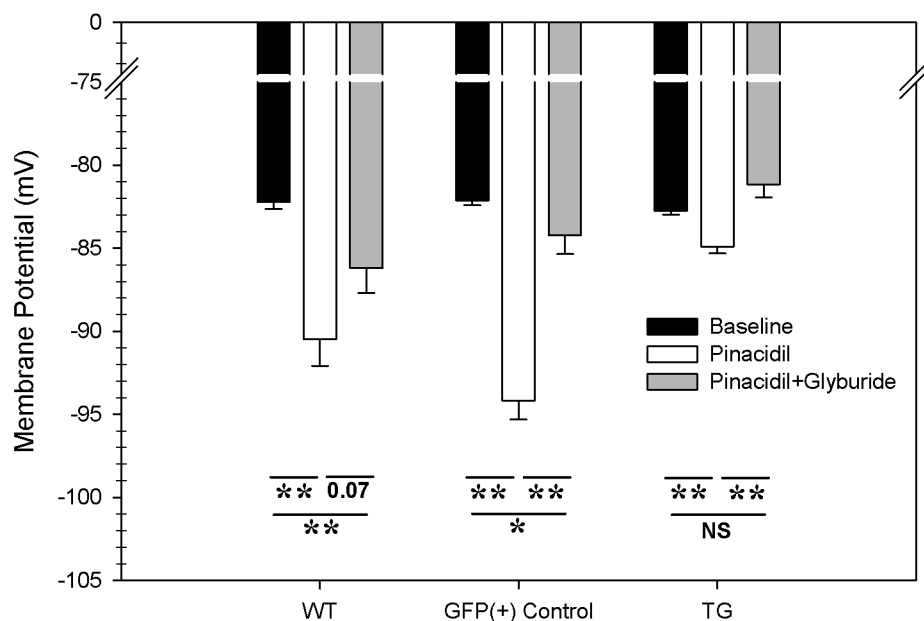
Figure 25. Membrane potential between WT, GFP(+), and TG groups for each step of the pinacidil protocol. (*p<0.05; **p<0.01)

Table 9. Two-sided, unpaired t-test values over membrane potential for pinacidil data shown in Figure 25. (*p<0.05; **p< 0.01)

	Baseline/Pinacidil	Baseline/Pin+Gly	Pin/Pin+Gly
WT	10^{-10} (**)	0.00079 (**)	0.075
GFP	10^{-21} (**)	0.024 (*)	10^{-7} (**)
TG	0.000018 (**)	0.15	0.0057 (**)
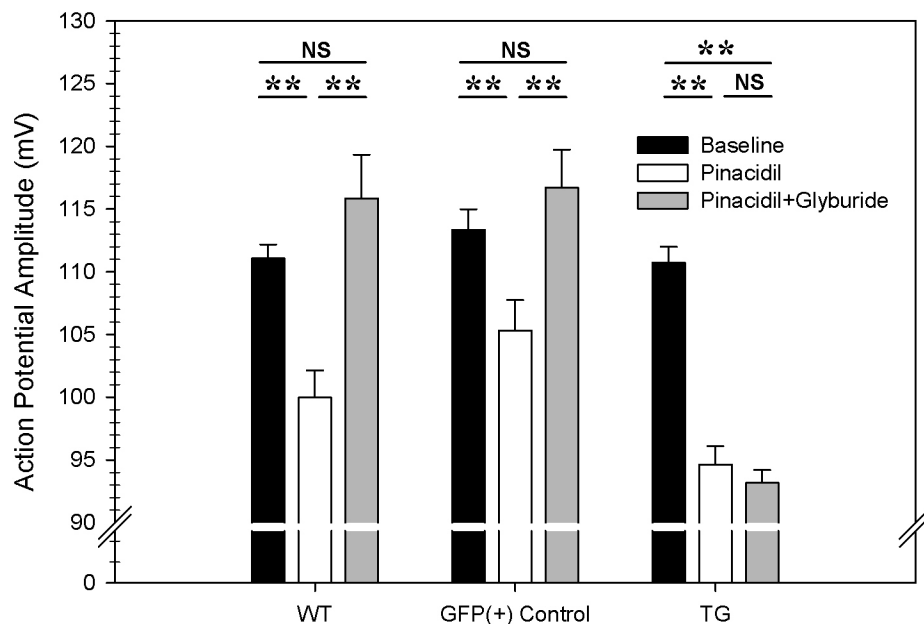
Figure 26. Action potential amplitude between WT, GFP(+), and TG groups for each
step of the pinacidil protocol. (*p<0.05; **p< 0.01)

Table 10. Two-sided, unpaired t-test values over action potential amplitudes for
pinacidil data shown in Figure 26. (*p<0.05; **p< 0.01)

	Baseline/Pinacidil	Baseline/Pin+Gly	Pinacidil/Pin+Gly
WT	0.0000033 (**)	0.094	0.00023 (**)
GFP	0.0086 (**)	0.30	0.0068 (**)
TG	10^{-11} (**)	0.0016 (**)	0.73
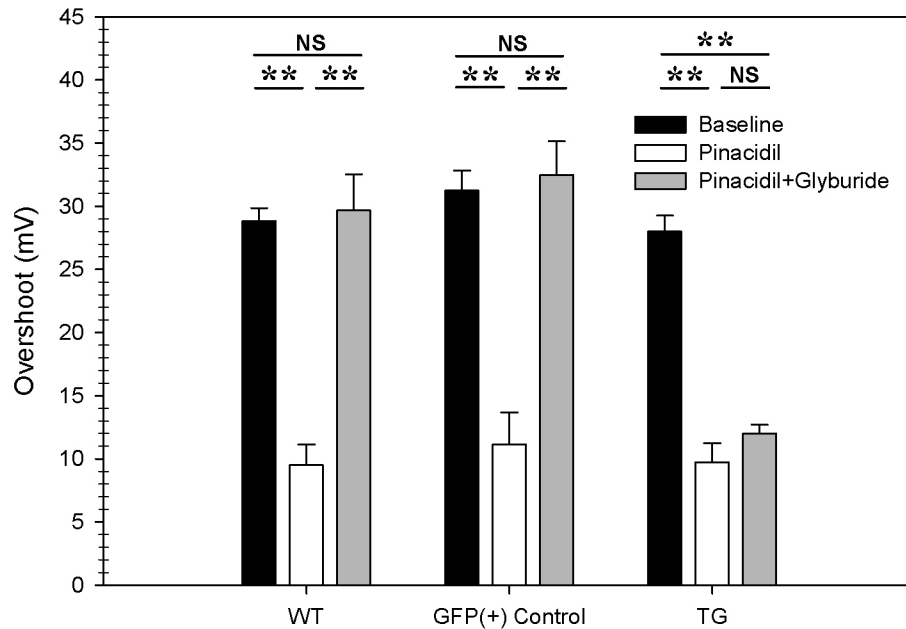
Figure 27. Overshoot between WT, GFP(+), and TG groups for each step of the pinacidil protocol. (*p<0.05; **p< 0.01)

Table 11. Two-sided, unpaired t-test values over overshoot for pinacidil data shown in Figure 27. (*p<0.05; **p< 0.01)

	Baseline/Pinacidil	Baseline/Pin+Gly	Pinacidil/Pin+Gly
WT	10^{-16} (**)	0.74	10^{-8} (**)
GFP	10^{-12} (**)	0.68	10^{-7} (**)
TG	10^{-12} (**)	0.0039 (**)	0.61

Table 12. Number of action potentials for WT, GFP(+), and TG groups and for each step of the pinacidil protocol including row and column totals.

	Baseline	Pinacidil	Pin+Gly	Totals
WT (N=19)	73	28	19	120
GFP (N=18)	50	23	26	99
TG (N=14)	50	24	3	77
Totals	173	75	48	296

Table 13. Summary of membrane potential (V_m), action potential amplitude (AP), and overshoot (V_o) as graphed in Figure 25, Figure 26, and Figure 27. (mean±SE)

		WT	GFP(+)	TG
Baseline	V_m	−82.23±0.42	−82.12±0.29	−82.74±0.25
	AP	111.07±1.10	113.35±1.64	110.73±1.27
	V_o	28.85±1.01	31.23±1.61	27.99±1.27
Pinacidil	V_m	−90.48±1.60	−94.17±1.15	−84.90±0.41
	AP	99.98±2.16	105.32±2.44	94.64±1.46
	V_o	9.94±1.65	11.15±2.53	9.74±1.50
Pinacidil + Glyburide	V_m	−86.19±1.50	−84.23±1.13	−81.17±0.78
	AP	115.85±3.47	116.71±3.01	93.17±1.04
	V_o	29.66±2.88	32.48±2.67	12.00±0.69

Table 14. One-way ANOVA over WT/GFP/TG for each step of the pinacidil protocol (baseline, twitched, glyburide) for each parameter (V_m, AP, V_o). (*p<0.05; **p<0.01)

	V_m	AP	V_o
Baseline	0.48	0.36	0.22
Pinacidil	10^{-5} (**)	0.0039 (**)	0.81
Pin+Gly	0.33	0.048 (*)	0.047 (*)

Table 15. One-way ANOVA over baseline/twitched/glyburide for mouse group (WT, GFP, TG) for each parameter (V_m, AP, V_o) of the pinacidil protocol. (*$p<0.05$; **$p<0.01$)

	V_m	AP	V_o
WT	10^{-9} (**)	10^{-6} (**)	10^{-15} (**)
GFP	≈ 0 (**)	10^{-4} (**)	10^{-10} (**)
TG	≈ 0 (**)	10^{-4} (**)	10^{-9} (**)

Table 16. Two-sided, unpaired t-test values pair-wise between groups for each step of the pinacidil protocol and parameter measured. (*$p<0.05$; **$p<0.01$)

		V_m	AP	V_o
Baseline	WT vs. GFP	0.85	0.24	0.19
	WT vs. TG	0.36	0.84	0.60
	GFP vs. TG	0.11	0.21	0.12
Twitched	WT vs. GFP	0.085	0.11	0.58
	WT vs. TG	0.76	0.46	0.87
	GFP vs. TG	10^{-9} (**)	0.00056 (**)	0.64
Glyburide	WT vs. GFP	0.30	0.86	0.49
	WT vs. TG	0.99	0.26	0.033 (*)
	GFP vs. TG	0.38	0.016 (*)	0.018 (*)

4.7 Endogenous action potentials in skeletal muscle

All analyzed action potentials have been the result of supramaximal stimulation of the sciatic nerve. Recordings were performed on anesthetized mice; some mice were more tolerant of the isoflurane. As with all anesthetics, there is a trade-off between depth of anesthesia and undesirable nervous system depression (e.g., death). In these tolerant mice, the level of isoflurane to meet the target respiratory rate was marginally insufficient to fully disengage motor neurons from the remainder of the central nervous system. This

lead to twitches of the TA that were not visually perceptible but were recordable with the force transducer and floating microelectrode. These action potentials have been designated as endogenous action potentials.

One recording of endogenous action potentials is shown in Figure 28. In Figure 28, three endogenous action potentials were recorded from a single impalement and were in fairly quick succession, but not sufficiently fast to produce summation of force twitches. The corresponding force twitches are shown in the left half of Figure 29 and, for comparison, a supramaximal exogenous force twitch shown in the right half. Other endogenous action potentials were observed (data not shown) that produced a summation of force twitches.
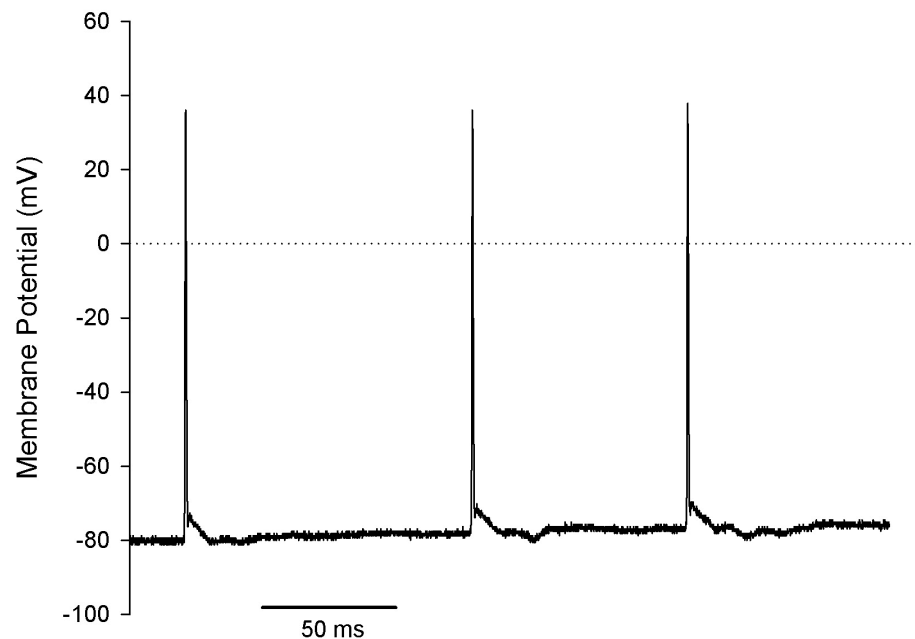
Figure 28. Three sequentially recorded endogenous action potentials from a single impalement.
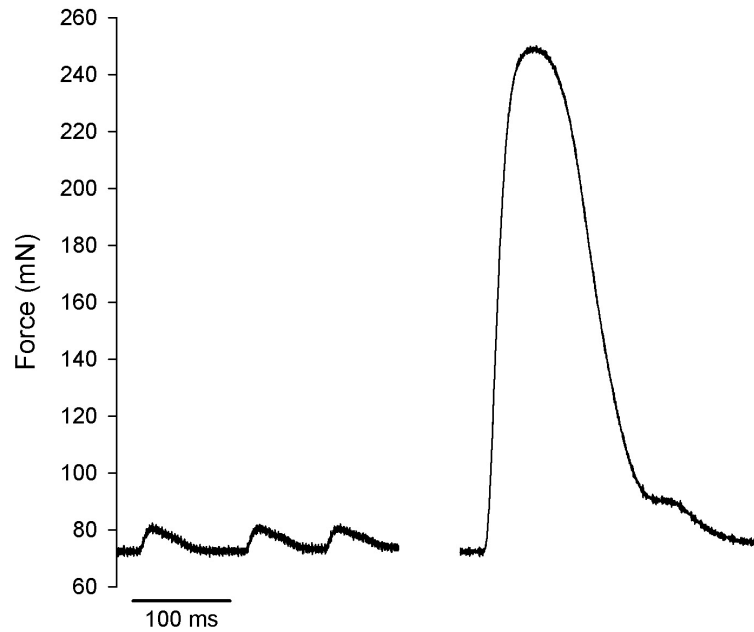
Figure 29. Three small force twitches (left) corresponding to endogenous action
potentials from Figure 28 and a supramaximally-stimulated exogenous force
twitch for comparison.

4.8 Delayed afterdepolarizations in skeletal muscle

Afterdepolarizations refer to a spontaneous depolarization of the heart either
during phase 3 ("early afterdepolarization" or EAD) or during phase 4 ("delayed
afterdepolarization" or DAD) after a non-spontaneous depolarization. This is believed to
be caused by calcium overload and an influx of sodium from the Na-Ca exchanger. (Katz
2006) Very little has been published on afterdepolarizations in skeletal muscle. DAD's
were recorded in WT, GFP(+), and TG mice with no apparent group specificity.

Figure 30 and Figure 31 show recordings of exogenous action potentials with
DAD's. In these figures, the electrically stimulated exogenous action potentials are
indicated with an asterisk and the DAD's are unmarked. Note that the membrane
potential leading up to the DAD's show a steady depolarization similar to that of the
sodium current in myogenic cardiomyocytes of the sinoatrial node that leads to
spontaneous depolarization.
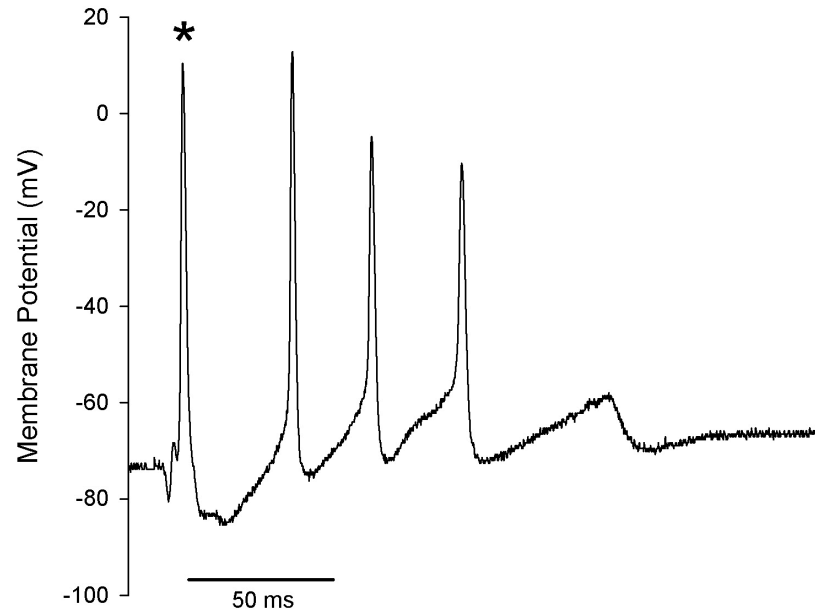
Figure 30. An action potential is denoted with an asterisk (*) and the three following peaks are believed to be delayed afterdepolarizations.
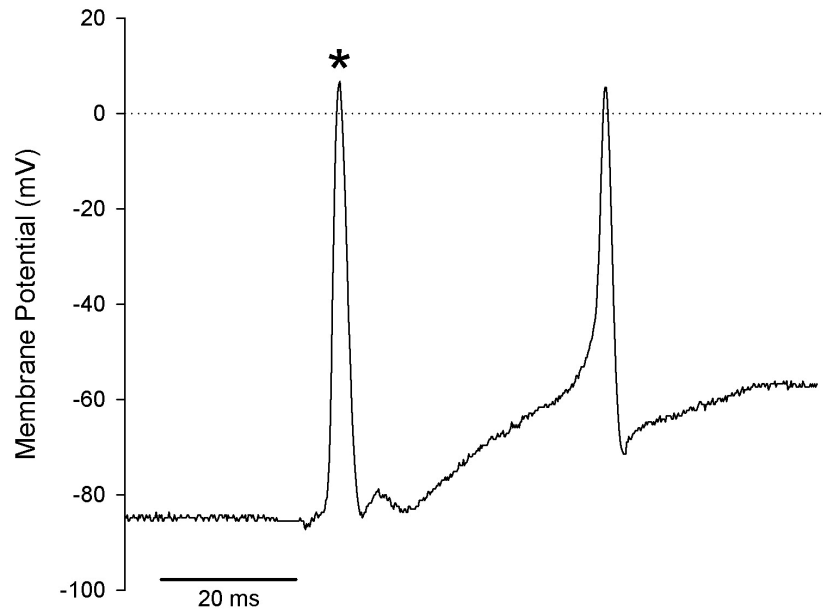
Figure 31. An action potential is denoted with an asterisk (*) and the following peak is believed to be a delayed afterdepolarization.

4.9 Giant action potentials in skeletal muscle

As shown previously, the amplitude of an action potential does not *appear* to be normally distributed (see Figure 19). Of action potential amplitudes, the sample mean was calculated as 103.2 mV and a standard deviation of 13.3 mV, which places the action potential shown in Figure 32 at 3.64 standard deviations from the mean. This giant action potential is the largest of all recorded action potentials. (The 5 mV hyperpolarization approximately 1 ms before the action potential is a stimulus artifact and can be ignored.) If the action potential amplitude *did* follow a normal distribution then the probability of an action potential occurring with amplitude 153.5 mV or larger would be 0.014%. This recording occurred with the same muscle and same FME tip as other "normal" action potentials.
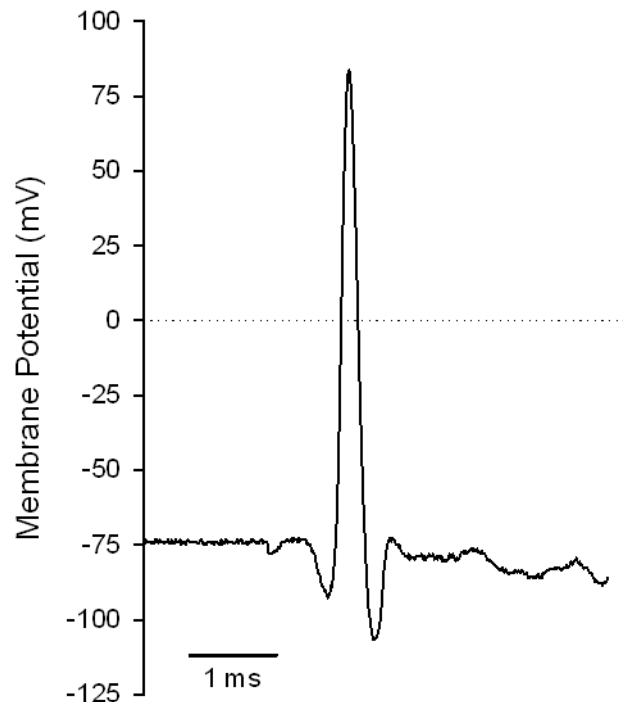
Figure 32. A giant action potential showing a membrane potential of −73.92 mV, an AP amplitude of 153.5 mV, and an overshoot of 80.57 mV.

CHAPTER 5

DISCUSSION

Maintenance of cellular energetic state is crucial for cells to survive. An integral component to any control system — biological or man-made — is the feedback loop. In striated muscle, the K_{ATP} channel acts as a negative feedback loop by hyperpolarization of the membrane to counter a reduction in energetic state (i.e., a reduction in the [ATP]/[ADP] ratio). In a lower energetic state, K_{ATP} channels open which permits potassium ions to move down their electrochemical gradient and this shifts the membrane potential more negative (toward V_K). For example, in beta cells, high blood glucose levels corresponds to high energetic state and closing of K_{ATP} channels, which leads to membrane instability to depolarize and the exocytosis of insulin (Seino, Takahashi et al. 2012). In skeletal muscle, a change in the state of K_{ATP} channels is manifested in changes to the morphology of action potentials.

5.1 Cardiac Muscle

In cardiac muscle, the duration of the action potential is significantly longer than in skeletal muscle by approximately two orders of magnitude. The duration of the cardiac action potential has been shown to reflect the internal energetic state. Figure 13 shows one such way that the action potential can be used as an indicator of the cellular energetic state. At a long pacing cycle length the workload on the heart is relatively low and decreasing the pacing cycle length increases the workload of the heart. After the 150-to-130 ms transition, there is an indistinguishable difference between ΔAPD_{90} of WT mice and Tg[αMHC-K_{ir}6.1AAA] mice even though the TG mice have an 80-85% reduction in functional K_{ATP} channels.

After the 130-to-100 ms transition, there are two separations in the groups of mice. The first is the exercised WT mice showed a significant reduction in APD_{90} and

also this parameter was reduced more quickly. The second is the WT mice exposed to glyburide showed the least reduction of all mice. Both support the negative feedback by K_{ATP} channels: increased expression from exercise exposure would promote shortening of the action potential, and pharmacologically closing channels would result in action potentials that do not respond to metabolic load. A reduction of K_{ATP} channels in TG models results in slowing of action potential response to energetic load and this reduces energetic efficiency.

After the 100-to-80 ms transition, the reduction in functional K_{ATP} channels in TG mice is more evident. Exercised and sedentary WT mice no longer have a significant difference at steady state unlike shown for the 130-to-100 ms transition. Additionally, the APD_{90} reduction for exercised WT is not as large as after the 130-to-100 ms transition. This work is supported by an increase in SUR2A expression, $K_{ir}6.2$ expression, channel density, K_{ATP} channel current, and an increase in oxygen consumption by TG mice at all three transitions (Zingman, Zhu et al. 2011). Increasing the workload is one way to change the energetic stress on cardiac muscle to understand how the action potential reflects these changes.

A more extreme way to test the energetic response of aerobic tissue is to place the tissue under hypoxia. Since the tissue is dependent upon a continuous supply of oxygen, then the removal of oxygen will have a fairly rapid effect. Oxygen is used in cellular respiration as the final electron acceptor in a long chain of reactions that creates ATP from ADP. Elimination of oxygen prevents ATP production and the [ATP]/[ADP] ratio decreases, thereby reducing the energetic state. Under these conditions, K_{ATP} channels open and shorten the action potential duration. In Figure 16, the WT and GFP(+) mice had similar responses and reached the same steady-state value as the TG mice. This suggests that the level of K_{ATP} channel expression in the tested range (15-150% nominal) does not alter the steady-state action potential duration during hypoxia, but rather the rate that steady state is achieved. If treated as an overdamped transient response then the

delay time can be used. The delay time is significantly longer for TG mice than either WT or GFP(+). As a feedback mechanism, opening of K_{ATP} channels when cellular energy is low reduces calcium entry that then reduces further energy expenditure. Hypoxia alters the morphology of the action potential that can be used to indicate that the cell is under energetic stress.

5.2 Skeletal Muscle

The primary focus of this work is on recording the membrane of skeletal muscle fibers *in situ*. To do this, an old technique — the floating microelectrode — was employed in a novel way. The use of a floating microelectrode permits direct measurement of the membrane potential as well as reducing motion artifacts. This presents an opportunity to record more physiologically accurate data than with either isolated or uncoupled fibers.

In one study (Gong, Legault et al. 2003) the range of V_m in isolated extensor digitorum longus (EDL) fibers was found to be −67 to −94 mV and another study (McKenna, Bangsbo et al. 2008) the range of unfatigued muscles had a range of −75 to −85 mV. As the result of stochastic processes, the membrane potential would be expected to follow a probability distribution and a range is insufficient to describe a distribution. In Figure 18, the membrane potential in unfatigued TA is shown to approximately follow a Normal(μ=−83.5, σ=3.8) distribution. The action potential exclusion thresholds placed upon data collection may be responsible for the skew. These thresholds clearly affect the distribution of both action potential amplitude and overshoot as shown in Figure 19 and Figure 20.

In a review by (McKenna, Bangsbo et al.), others have shown that fatigue alters the membrane potential. By increasing $[K^+]_o$ and decreasing $[K^+]_i$, the V_K increases leading to depolarization; sodium and potassium have opposing gradients, so the decrease in $[Na^+]_o$ and the increase in $[Na^+]_i$ serve to hyperpolarize the membrane; and a possible

increase in $[Cl^-]_i$ would lead to a depolarization of the membrane. Overall, an inactivation in Na^+ channels leads to reduction of action potential amplitude, and a decline in Na^+/K^+ ATPase activity contributes to fatigue. Fatigue appears to be a multifactorial result of repetitive contractions.

Routine daily activity is unlikely to be fatigue inducing and previous studies of skeletal muscle have used fatigue-inducing protocols. Therefore, to better understand the involvement of K_{ATP} channels in routine skeletal muscle activity a non-fatiguing protocol was used. Physiological twitching of 1 Hz was employed with TA muscles. From this, Figure 21 shows that this twitching induces a significant reduction in the membrane potential in WT and GFP(+) but not Tg[MyoD-K_{ir}6.1AAA] mice. This hyperpolarization was reversed by superfusion of glyburide. This suggests that this hyperpolarization is due to K_{ATP} channels. Additionally, this was confirmed without the 1 Hz twitching through the use of the K_{ATP} channel opener pinacidil, shown in Figure 25. The non-response of action potential amplitude agrees with (McKenna, Bangsbo et al. 2008) that the decrease in amplitude is due to Na^+ channels. Finally, since membrane potential, action potential amplitude, and overshoot are interrelated ($V_m + AP = V_o$) there are only two degrees of freedom and the changes in overshoot are due to those seen in membrane potential and action potential amplitude. One possible confounding variable is that the K_{ATP} channel expression differs between oxidative and glycolytic fibers (Banas, Clow et al. 2011) and may develop different distributions based upon fiber type.

During the course of recording data for the previously discussed results, some unusual action potentials were recorded. The first is the so-called endogenous action potentials. As expected, these action potentials show a similar membrane potential and action potential amplitude as exogenous action potentials. The three endogenous action potentials shown in Figure 28 have a twitch force of about 4% of a supramaximal twitch (as shown in Figure 29). This suggests 4% of the motor neurons were activated including the impaled muscle fiber. The recording of numerous other force twitches without action

potentials (data not shown) supports this notion that only a small number of motor neurons were activated and may represent fasciculations. The second is the so-called delayed afterdepolarizations. Due to the shortness of the action potential of skeletal muscle, the only likely afterdepolarizations to be recorded are delayed afterdepolarizations (DAD's). All recorded afterdepolarizations have been DAD's and have been recorded in various qualities including many indistinguishable from motion artifacts. These DAD's could also be a secondary finding to cellular injury from the ME impalement that leads to leak of ions and loss of membrane potential. However, the clarity of some recordings suggests Figure 30 and Figure 31 are not motion artifacts, as they also exhibit myogenic-like slow depolarization found along the conduction path in the heart. The third is the so-called giant action potential. The small likelihood of an action potential having this amplitude suggests that the recording in Figure 32 is not likely to be a normal skeletal myocyte action potential. However, using the same FME tip on the same muscle within seconds of a normal membrane and action potentials strongly supports that this giant action potential is not due to technical nor electronic error. The FME tip could be impaled into a t-tubule or an organelle (e.g., sarcoplasmic reticulum) or in an entirely different excitable cell with different ion composition (e.g., satellite cell, neuron). Its genesis, still, is enigmatic since the amplitude is more positive than V_K, V_{Na}, and V_{Cl}, but not V_{Ca}.

CHAPTER 6

CONCLUSION

The energetic state of striated muscle can be revealed through detectable morphological changes in the action potential. An increase in K_{ATP} channels reveals a faster and stronger action potential response to an increase in workload in cardiac muscle; a faster action potential response to hypoxia in cardiac muscle; a depression of the membrane potential in skeletal muscle; and reduction in action potential amplitude in skeletal muscle. All of these changes act as a negative feedback signal to the cell that reduces further energy usage. In contrast, blockage or reduction in K_{ATP} channels has the opposite effect, leading to action potential changes that exacerbate energy utilization under energetic stress.

Reduction of energy use in cardiac muscle is important to preserve cardiac function when under energetic stress such as during a myocardial infarction. Reduction of energy use in skeletal muscle is also a mechanism to preserve energy efficiency. Tissue-specific disruption — possibly through changes in K_{ATP} channel expression — of this energy efficiency in skeletal muscle, but not cardiac muscle, may be a viable vector to naturally increase energy consumption and, thus, may be a useful bariatric intervention.

REFERENCES

Alekseev, A. E., S. Reyes, et al. (2010). "Sarcolemmal ATP-sensitive K(+) channels control energy expenditure determining body weight." Cell Metab **11**(1): 58-69.

Anandacoomarasamy, A., I. Caterson, et al. (2008). "The impact of obesity on the musculoskeletal system." Int J Obes (Lond) **32**(2): 211-222.

Banas, K., C. Clow, et al. (2011). "The KATP channel Kir6.2 subunit content is higher in glycolytic than oxidative skeletal muscle fibers." Am J Physiol Regul Integr Comp Physiol **301**(4): R916-925.

Barness, L. A., J. M. Opitz, et al. (2007). "Obesity: genetic, molecular, and environmental aspects." Am J Med Genet A **143A**(24): 3016-3034.

Barrett-Jolley, R., A. Comtois, et al. (1996). "Effect of adenosine and intracellular GTP on KATP channels of mammalian skeletal muscle." J Membr Biol **152**(2): 111-116.

Bienengraeber, M., T. M. Olson, et al. (2004). "ABCC9 mutations identified in human dilated cardiomyopathy disrupt catalytic KATP channel gating." Nat Genet **36**(4): 382-387.

Blair, S. N., H. W. Kohl, 3rd, et al. (1995). "Changes in physical fitness and all-cause mortality. A prospective study of healthy and unhealthy men." JAMA **273**(14): 1093-1098.

Chen, J. C., J. Mortimer, et al. (2005). "MyoD-cre transgenic mice: a model for conditional mutagenesis and lineage tracing of skeletal muscle." Genesis **41**(3): 116-121.

Cifelli, C., F. Bourassa, et al. (2007). "KATP channel deficiency in mouse flexor digitorum brevis causes fibre damage and impairs Ca2+ release and force development during fatigue in vitro." J Physiol **582**(Pt 2): 843-857.

Curley, M., M. T. Cairns, et al. (2002). "Expression of mRNA transcripts for ATP-sensitive potassium channels in human myometrium." Mol Hum Reprod **8**(10): 941-945.

de Ferranti, S. and D. Mozaffarian (2008). "The perfect storm: obesity, adipocyte dysfunction, and metabolic consequences." Clin Chem **54**(6): 945-955.

Flagg, T. P., D. Enkvetchakul, et al. (2010). "Muscle KATP channels: recent insights to energy sensing and myoprotection." Physiol Rev **90**(3): 799-829.

Franz, M. R., D. Burkhoff, et al. (1986). "In vitro validation of a new cardiac catheter technique for recording monophasic action potentials." Eur Heart J **7**(1): 34-41.

Fraser, J. A. and C. L. Huang (2007). "Quantitative techniques for steady-state calculation and dynamic integrated modelling of membrane potential and intracellular ion concentrations." Prog Biophys Mol Biol **94**(3): 336-372.

Garlid, K. D. and A. P. Halestrap (2012). "The mitochondrial K(ATP) channel-Fact or fiction?" J Mol Cell Cardiol.

Gong, B., D. Legault, et al. (2003). "KATP channels depress force by reducing action potential amplitude in mouse EDL and soleus muscle." Am J Physiol Cell Physiol **285**(6): C1464-1474.

Gromada, J., X. Ma, et al. (2004). "ATP-Sensitive K+ Channel-Dependent Regulation of Glucagon Release and Electrical Activity by Glucose in Wild-Type and SUR1-/- Mouse Alpha-Cells." Diabetes **53**(suppl_3): S181-S189.

Halliwell, J., M. Whitaker, et al. (1987). Using Microelectrodes. Microelectrode Techniques. D. Ogden. Cambridge, UK, Company of Biologists Limited**:** 1-11.

Harper, J. A., K. Dickinson, et al. (2001). "Mitochondrial uncoupling as a target for drug development for the treatment of obesity." Obesity Reviews **2**(4): 255-265.

Haslam, D. W. and W. P. James (2005). "Obesity." Lancet **366**(9492): 1197-1209.

Hille, B. (2001). Ion Channels of Excitable Membranes. Sunderland, MA, Sinauer Associates.

Holmuhamedov, E. L., A. Jahangir, et al. (2004). "Potassium channel openers are uncoupling protonophores: implication in cardioprotection." FEBS Lett **568**(1-3): 167-170.

Kane, G. C., A. Behfar, et al. (2006). "KCNJ11 gene knockout of the Kir6.2 KATP channel causes maladaptive remodeling and heart failure in hypertension." Hum Mol Genet **15**(15): 2285-2297.

Kane, G. C., A. Behfar, et al. (2004). "ATP-Sensitive K+ Channel Knockout Compromises the Metabolic Benefit of Exercise Training, Resulting in Cardiac Deficits." Diabetes **53**(suppl_3): S169-S175.

Kane, G. C., X. K. Liu, et al. (2005). "Cardiac KATP channels in health and disease." J Mol Cell Cardiol **38**(6): 937-943.

Katz, A. M. (2006). Physiology of the Heart. Philadelphia, PA, Lippincott Williams & Wilkins.

Kovacs, M., J. Toth, et al. (2004). "Mechanism of blebbistatin inhibition of myosin II." J Biol Chem **279**(34): 35557-35563.

Ling, G. and R. W. Gerard (1949). "The normal membrane potential of frog sartorious fibers." J Cell Physiol **34**(3): 383-396.

Malester, B., X. Tong, et al. (2007). "Transgenic expression of a dominant negative K(ATP) channel subunit in the mouse endothelium: effects on coronary flow and endothelin-1 secretion." FASEB J **21**(9): 2162-2172.

McKenna, M. J., J. Bangsbo, et al. (2008). "Muscle K+, Na+, and Cl disturbances and Na+-K+ pump inactivation: implications for fatigue." J Appl Physiol **104**(1): 288-295.

Miki, T., K. Nagashima, et al. (1998). "Defective insulin secretion and enhanced insulin action in KATP channel-deficient mice." Proc Natl Acad Sci U S A **95**(18): 10402-10406.

Noma, A. (1983). "ATP-regulated K+ channels in cardiac muscle." Nature **305**(5930): 147-148.

Park, Y. B., Y. J. Choi, et al. (2011). "ATP-Sensitive Potassium Channel-Deficient Mice Show Hyperphagia but Are Resistant to Obesity." Diabetes Metab J **35**(3): 219-225.

Popkin, B. M., L. S. Adair, et al. (2012). "Global nutrition transition and the pandemic of obesity in developing countries." Nutr Rev **70**(1): 3-21.

Quesada, I., J. M. Rovira, et al. (2002). "Nuclear KATP channels trigger nuclear Ca(2+) transients that modulate nuclear function." Proc Natl Acad Sci U S A **99**(14): 9544-9549.

Røed, A. (1993). "Excitation-contraction uncoupling in the rat diaphragm by 2,3-butanedione monoxime." European Journal of Pharmacology **241**(2-3): 229-236.

Rubio-Cabezas, O., T. Klupa, et al. (2011). "Permanent neonatal diabetes mellitus--the importance of diabetes differential diagnosis in neonates and infants." Eur J Clin Invest **41**(3): 323-333.

Seino, S. and T. Miki (2003). "Physiological and pathophysiological roles of ATP-sensitive K+ channels." Prog Biophys Mol Biol **81**(2): 133-176.

Seino, S., H. Takahashi, et al. (2012). "Treating diabetes today: a matter of selectivity of sulphonylureas." Diabetes Obes Metab **14 Suppl 1**: 9-13.

Sjostrom, L., A. K. Lindroos, et al. (2004). "Lifestyle, diabetes, and cardiovascular risk factors 10 years after bariatric surgery." N Engl J Med **351**(26): 2683-2693.

Solomon, C. G. and R. G. Dluhy (2004). "Bariatric surgery--quick fix or long-term solution?" N Engl J Med **351**(26): 2751-2753.

Spriet, L. L. and M. Hargreaves (2006). Overview of Exercise Metabolism. Exercise Metabolism. Champaign, Illinois, Human Kinetics**:** 1-7.

Standen, N. B., A. I. Pettit, et al. (1992). "Activation of ATP-dependent K+ currents in intact skeletal muscle fibres by reduced intracellular pH." Proc Biol Sci **247**(1320): 195-198.

Sturm, R. (2007). "Increases in morbid obesity in the USA: 2000-2005." Public Health **121**(7): 492-496.

Tainter, M. L., W. C. Cutting, et al. (1934). "Use of Dinitrophenol in Nutritional Disorders: A Critical Survey of Clinical Results." Am J Public Health Nations Health **24**(10): 1045-1053.

Tong, X., L. M. Porter, et al. (2006). "Consequences of cardiac myocyte-specific ablation of KATP channels in transgenic mice expressing dominant negative Kir6 subunits." Am J Physiol Heart Circ Physiol **291**(2): H543-551.

Virgili, N., J. F. Espinosa-Parrilla, et al. (2011). "Oral administration of the KATP channel opener diazoxide ameliorates disease progression in a murine model of multiple sclerosis." J Neuroinflammation **8**: 149.

Widmaier, E. P., H. Raff, et al. (2008). Vander's Human Physiology, McGraw-Hill.

Yamada, K., J. J. Ji, et al. (2001). "Protective role of ATP-sensitive potassium channels in hypoxia-induced generalized seizure." Science **292**(5521): 1543-1546.

Yan, F. F., Y. W. Lin, et al. (2007). "Congenital hyperinsulinism associated ABCC8 mutations that cause defective trafficking of ATP-sensitive K+ channels: identification and rescue." Diabetes **56**(9): 2339-2348.

Yang, S.-G. and O. Kittnar (2010). "New insights into application of cardiac monophasic action potentials." Physiological Research **59**(5): 645-650.

Yee, K. K., S. K. Sukumaran, et al. (2011). "Glucose transporters and ATP-gated K+ (KATP) metabolic sensors are present in type 1 taste receptor 3 (T1r3)-expressing taste cells." Proc Natl Acad Sci U S A **108**(13): 5431-5436.

Yensen, C., W. Matar, et al. (2002). "K+-induced twitch potentiation is not due to longer action potential." Am J Physiol Cell Physiol **283**(1): C169-177.

Zhu, Z., C. M. Burnett, et al. (2011). "Reduction in number of sarcolemmal KATP channels slows cardiac action potential duration shortening under hypoxia." Biochem Biophys Res Commun **415**(4): 637-641.

Zingman, L. V., D. M. Hodgson, et al. (2002). "Kir6.2 is required for adaptation to stress." Proc Natl Acad Sci USA **99**(20): 13278-13283.

Zingman, L. V., Z. Zhu, et al. (2011). "Exercise-induced expression of cardiac ATP-sensitive potassium channels promotes action potential shortening and energy conservation." J Mol Cell Cardiol **51**(1): 72-81.

APPENDIX A. RECIPES

The following are recipes for various solutions used throughout the experiments. All of these solutions are well established and are reproduced here mostly for convenience.

Krebs-Henseleit Solution is a solution that mimics the extracellular concentrations and includes buffers. The Krebs-Henseleit requires preparation to the desired pH while being bubbled with 95% O_2/5% CO_2 and heated to the desired temperature. The final solution is 320 Osm at a pH of 7.4 at 37.4°C. Alternatively, the solution can be bubbled with 95% N_2/5% CO_2 for inducing hypoxia.

- 143.5 mM Na^+
- 5.9 mM K^+
- 2.5 mM Ca^{2+}
- 1.2 mM Mg^{2+}
- 1.2 mM $(PO_4)^{3-}$
- 128 mM Cl^-
- 25 mM HCO^{3-}
- 11 mM Glucose
- No insulin

Mix reagents in order to 800 mL water, cover and bubble 95% O_2/5% CO_2, add HCl to pH 7.4, and fill to 1000 mL in graduated cylinder. Cover, bubble, heat to 37.4°C, and adjust pH to 7.4. Filter.

Tyrode's Solution is a solution that mimics the extracellular concentrations and includes a buffer. This solution does not require bubbling and is easier to work with than Krebs-Henseleit. The final solution is 292 Osm at a pH of 7.4 at 31°C. Alternatively, the solution can include 10 µM glyburide, 100 µM pinacidil, or both glyburide plus pinacidil.

- 136 mM Na^+

- 5.4 mM K^+

- 5.5 mM HEPES

- 0.53 mM Mg^{2+}

- 0.45 mM Ca^{2+}

- 144 mM Cl^-

- No glucose

- No insulin

Mix HEPES and 0.6 g Chelex 100 Na in 800 mL water for 15 minutes then filter. Mix in NaCl and KCl then filter. Adjust pH to 7.2 with NaOH, dilute to 1000 mL in graduated cylinder, re-adjust pH, then filter. Refrigerate as 10x stock. Dilute to 1x (e.g., 25 mL 10x stock in 225 mL water) and mix in $MgCl_2$ and $CaCl_2$ then adjust pH to 7.4.

Avertin is the trade name of a 2,2,2-tribromoethanol-based anesthetic once manufactured by Winthrop Laboratories. No longer commercially produced, it must be made from ingredients. The final mass concentration is 2.5 g/10 mL.

- 1 g of 2,2,2-tribromoethanol

- 1 mL of 2-methyl-2-butanol (t-amyl alcohol)

Mix tribromoethanol in t-amyl alcohol at 37°C for 100% stock. Dilute to 2.5% by mixing with water or normal saline to get 2.5 g per 10 mL (e.g., 50 μL into 2 mL water).

Glyburide (USAN) is a K_{ATP} channel closer and alternatively known as glibenclamide (INN). Glyburide is a sulfonylurea and interacts with the SUR1, SUR2A, and SUR2B subunits of K_{ATP} channels. The final solution is 10 μM of glyburide.

- 19.76 mg of glyburide (FW 494.01 g/mol)

- 400 μL of DMSO

Mix glyburide and DMSO to make 0.1M stock, then dilute with DMSO to 10 μM (e.g., 10 μL in 100 mL DMSO).

Pinacidil is a K_{ATP} channel opener and is a member of the cyanoguanidine class of drugs. The final solution is 100 μM of pinacidil.

- 20.00 mg of pinacidil monohydrate (FW 263.34 g/mol)
- 760 μL of DMSO

Mix pinacidil and DMSO to make 0.1M stock, then dilute with DMSO to 100 μM (e.g., 100 μL in 100 mL DMSO).

APPENDIX B. PROTOCOLS

For the experiment using the MAP electrode that looked at transient responses to changes in pacing cycle length, some mice from both WT and TG groups were exposed to exercise on a treadmill (Columbus Instruments; Columbus, OH) while others remained sedentary. For each of three days of a training period, the mice were acclimated to the non-moving treadmill for 45 minutes and then exposed to 15 minutes of moving at 3.5 m/min. For each of the next five days, the mice were put on the treadmill for 45 minutes of moving at 12 m/min at an inclination of 15°. On the last day (day 8), the mice were sacrificed.

For the *in situ* study of the tibialis anterior (TA) muscle using the floating microelectrode, the mice were first anesthetized with avertin. The skin and muscle fascia were dissected away with a dissection microscope and then the mouse was transferred to the *in situ* apparatus, placed under isoflurane, and superfusion of Tyrode's solution was started. The mouse was secured to the apparatus through a 30G 1-1/2" needle and to the force transducer with 3/0 silk suture. Platinum wires were introduced in proximity to the sciatic nerve. Once everything was set, then the electrophysiological protocol was started.

The first step was to set the force transducer to isometric and fix the passive tension to 75 mN. After numerous trials on difference mice, 75 mN was found to consistently produce nearly the maximum twitch force (F_{max}) on the force-length curve. There were two confounding issues to the traditional approach to finding F_{max}:

1. Although the distal tendon of the TA was sutured to the force transducer, the force recording is not purely a result of twitches in the TA as the sciatic innervates other muscles.

2. Due to different lengths of suture used, then the length measured by the force transducer is essentially arbitrary.

The second step was to set the stimulus isolation unit (SIU) to cause a supramaximal stimulation of the TA. This was done by twitching in pCLAMP at 1 Hz and adjusting the current on the SIU until maximum force was produced. Generally, for the platinum electrode used this was found to be approximately 10% of 10 mA, or 1 mA. If the maximum value was significantly higher (>20%) then the platinum wires were relocated and this step was repeated only once to avoid possible damage to the sciatic nerve. Once the maximum was found, this value was increased by 6-10%.

The third step was to measure the "baseline" membrane potential. First, the "zero offset" was adjusted to zero using pCLAMP's membrane test. Then the baseline measurement was performed with a gap-free recording in pCLAMP and manually twitching the TA after impaling the muscle.

The fourth step was to twitch the muscle at 1 Hz for 7 minutes. At minutes 5, 6, and just before 7 the muscle was impaled to record action potentials. This step was repeated a second time.

The fifth step was to superfuse the TA with 10 μM glyburide for 20 minutes.

The sixth step was to repeat the twitching and recording protocol from the fourth step by now with the TA exposed to glyburide. The twitching was repeated a second time as it was in the fourth step.

The seventh step was a 20-minute washout.

Finally, if the mouse and muscle were still healthy then this process was repeated a second time.

The above protocol is reused for the pinacidil experiments, but instead of twitching the K_{ATP} channel opener pinacidil is used instead. After taking a baseline measurement, 20 minutes of 100 μM pinacidil was superfused on the TA and a measurement was taken as was done for the baseline measurement (gap-free, manual twitching). Then 100 μM pinacidil + 10 μM glyburide was superfused and a final measurement was taken as was done for the baseline measurement.

APPENDIX C. MATLAB CODE

The following is a selection of MATLAB code for MAP analysis and is not intended to be complete but only to highlight how action potentials were parameterized. Input and output files are tab-delimited ASCII files and are unremarkable so all file handling is excluded.

```matlab
function [apddat, M, transitions, Fs] = APD90(fname, linestart, lineend, stimulation_periods, type, sedentary, label)
% Pulls out action potential duration for each AP between the given times
%               fname = file name of the tab-delimited file to read
%           linestart = line number in the file to start reading from
%             lineend = line number in the file to stop reading at
% stimulation_periods = Vector of stimulation periods to search for
%                type = Mouse type ('TG', 'GFP', 'WT')
%           sedentary = Determines if exercise or sedentary: 0=exercise, 1=sedentary
%               label = text appended to the end if not empty
%
% Returns a multitude of data
%      apddat = An Nx9 of APD information (see APDProcess.m)
%           M = Entire data set read in from fname
% transitions = An Mx2 of stimulation transitions (see APDTransitions.m)
%          Fs = Sampling frequency as determined by the difference in the
%               first column of the first two samples

% ------------------------------ LOADING ------------------------------

% This is Excel-like notation where A & C get 1st through 3rd columns
% and the numbers indicate the line numbers to read
%
% These files have a 22 header in them so skip them
range = strcat('A', int2str(22+linestart), '..', 'C', int2str(23+lineend));

% Read in the data
M = dlmread(fname, '\t', range);


% Append label to end if supplied
if ~isempty(label)
    fnamelen = length(fname);
    fname = strcat([fname(1:fnamelen-4), ' - ', label, fname(fnamelen-3:fnamelen)]);
end

% ------------------------------ PREPROCESS ------------------------------

% Get number of samples at Fs
L = length(M);

% Determine sampling rate (assuming uniform sampling rate)
% as the inverse of the first period in the data set
Fs = uint32(1/(M(2,1) - M(1,1)));

% Get just the action potential column
AP = M(1:L, 3);

% ------------------------------ CRUNCHING ------------------------------

% Segment the AP sequence
% One row per AP:
% [1] = Index in AP that the action potential starts
% [2] = Duration of action potential in AP
periods = APSegment(AP);

% Process AP's to get more information
% Do APD90 so 0.9
apddat = APDProcess(AP, periods, 0.9);

% Find the transitions
if ~isempty(stimulation_periods)
    transitions = APDTransitions(apddat, stimulation_periods);
else
    transitions = [];
end

% ---- Save as output file as desired ----
end
```

```matlab
function periods = APSegment(AP)
% Segment a series of action potentials
% and returns an Nx2 matrix of AP data of their starting index
% in AP and the AP period


% Take velocity derivative
dAP = diff(AP);

% Find where slope is generally the same before changes
movavg = filter([.25 .25 .25 .25], 1, dAP);
movavg = abs(movavg);

% Threshold of @movavg to assume an AP
thresh = .02;

% Find all possible starts of an action potential
starts = movavg > thresh;

% Do a moving average of 100 @starts and find where values are unity
% and this should be the start of the AP
startsavg = filter(ones(1,50), 1, starts) >= 1;


% Count number of AP's to know how much to pre-allocate for @periods
foundstart = 0;
APcount = 0;
for i = 1:length(startsavg)
    % Find where @startsavg changes to one
    % and use @foundstart to distinguish between first ==1 and last
    % ==1 in a given AP
    if startsavg(i) == 1
        if foundstart == 0
            foundstart = 1;
            APcount = APcount + 1;
        end
    % End of AP range
    elseif startsavg(i) == 0
        foundstart = 0;
    end
end

% Pull out period information
periods = zeros(APcount, 2);
foundstart = 0;
idx = 1; % Index in @periods to set new data to
for i = 1:length(startsavg)
    if startsavg(i) == 1
        if foundstart ~= 1
            foundstart = 1;

            periods(idx, 1) = i; % Index of start of this period

            % Find previous AP start index
            if idx > 1
                prev = periods(idx-1, 1);

                % Difference in start indices gives the total AP duration time (which should match that of the pacing)
                periods(idx-1, 2) = i - prev;
            else
                periods(idx, 2) = 0;
            end

            idx = idx + 1; % Fill in next index in @periods
        end
    % End of AP range
    elseif startsavg(i) == 0
        foundstart = 0;
    end
end


end


function apddat = APDProcess(AP, periods, APDpercent)
% Process the action potentials in AP with their periods given
% in an Mx2 matrix of one row per AP and [1] = starting index in AP; [2] =
% duration of AP.
%
% APDpercent is a value on (0, 1.0) that is the percent
% difference between baseline and maximum to count the APD for.
% For example, 0.9 would measure the APD90 and would be the duration of the
% AP that spans 90% down from maximum to baseline.
%
% Returns an Nx8 matrix with one row per AP:
% [1] = Index
% [2] = AP period
% [3] = Determine baseline average by using the end of the previous AP
% [4] = Determine max amplitudes relative to baseline
% [5] = Determine APD% value relative to baseline
% [6] = APD% duration
% [7] = APD% duty cycle
% [8] = APD% duration start index (absolute, not relative to [1])
% [9] = APD% duration end index (absolute, not relative to [1])
```

```
% Create space for APD data:
% [1] = Index
% [2] = AP period
% [3] = Determine baseline average by using the end of the previous AP
% [4] = Determine max amplitudes relative to baseline
% [5] = Determine APD% value relative to baseline
% [6] = APD% duration
% [7] = APD% duty cycle
% [8] = APD% duration start index (absolute, not relative to [1])
% [9] = APD% duration end index (absolute, not relative to [1])
apddat = zeros(length(periods), 9);

idx = 2;

% First and last periods are always garbage so start on two and go through
% length-1
for i = 2:length(periods)-1
    pstart = periods(i,1);
    pdur = periods(i,2);
    pend = pstart + pdur - 1;

    % Find the baseline interval start and end indexes
    iend = pstart;
    idur = 20;
    istart = iend - idur + 1;

    % Pull out the individual AP signal part
    theAP = AP(pstart:pend);

    % Average the 20 samples prior to this AP and use that as the baseline
    avg = sum(AP(istart:iend))/double(idur);

    apddat(idx, 1) = pstart;
    apddat(idx, 2) = pdur;
    apddat(idx, 3) = avg;
    apddat(idx, 4) = max(theAP) - apddat(idx,3);
    apddat(idx, 5) = (1-APDpercent) * apddat(idx,4);

    % Get the APD90 threshold and indices relative to @pstart
    [apd90, apd90first, apd90last] = APDthreshold(theAP, apddat(idx,3), apddat(idx,5));

    apddat(idx, 6) = apd90(1);
    apddat(idx, 7) = apddat(idx,6) / apddat(idx,2);
    apddat(idx, 8) = apd90first + pstart;
    apddat(idx, 9) = apd90last + pstart;

    idx = idx + 1;
end

end


function [APD, first, last] = APDthreshold(dat, baseline, thresh)
%   APDthreshold(data, baseline, threshold)
%
% Determine the APD duration by using the @dat assuming
% a baseline value of @baseline and a threshold value of @thrsh
% above this baseline

val = baseline + thresh;

% Shift zero line to that of the threshold
% All points that are now positive are candidates for the APD
dat = dat - val;

% Find all points that are positive, which means above the
% baseline+threshold and are those points considered to be of that APD
% threshold
points = find(dat > 0);

% No points means bad AP so no APD
if isempty(points)
    APD = 0;
    first = 0;
    last = 0;
else
    first = 0;
    last = 0;

    % Find the last continuous block of points
    prev = 0;
    for i=1:length(points)
        pt = points(i);

        % Assume the last bits are due to stimulus so disregard those
        if pt > length(dat)-15
            break
        end

        % Always set first and if there is jump then (pt-prev)>1
        % after 50 samples, assume the start has definitely started so
        % disregard starts after that (this is the case where the falling
        % edge of the AP dips beneath the threshold then jumps back up then
        % down again leading to an APD90 of only a few samples or zero)
        if first == 0 || (pt - prev > 1 && i < 20)
```

```matlab
            first = pt;
        end

        % Last point in contiguous block
        last = pt;

        % Keep track of previous point
        prev = pt;
    end

    APD = last - first;
end

end


function transitions = APDTransitions(apddat, expected_periods)
% Find the stimulation transitions as indicated in expected_periods
% which is a vector of AP periods in number of samples
%
% Returns a Mx2 matrix of [1] = AP start index; [2] = transitioned-to period

transitions = [];
prevtrans = 1;
for i = 1:length(expected_periods)
    % Count within a certain tolerance
    ediff = 3;

    for k = prevtrans:length(apddat)
        % Check the two subsequent AP's to make sure the transition has
        % occurred and not just a random bad AP prior to the actual
        % transition
        if abs(expected_periods(i) - apddat(k, 2)) <= ediff && abs(expected_periods(i) - apddat(k+1, 2)) <= ediff &&
abs(expected_periods(i) - apddat(k+2, 2)) <= ediff
                % Expanding is only done maybe 5 times, MATLAB doesn't know
                % that though so it's warning about it

                % Record expected period not actual period as it may
                % deviate within the tolerance
                transitions = [transitions; [k, expected_periods(i)]];

                prevtrans = k;
                break
        end
    end
end

end
```

APPENDIX D. SILVER CHLORIDING

Silver chloriding of silver wire is necessary to create a good, stable electrode. A desired length of silver wire is immersed into 3 mol/L potassium chloride with a solid piece of 25 x 25 x 2 mm 99.9985% silver foil (Cat. No. 12129; Alfa Aesar). A ±12 VDC power supply is used to alternate anode/cathode of the foil and wire. Periodic alternation of current applies or removes AgCl to the wire.

The power supply is connected to a single-pole, double-throw (SPDT) switch to +12 and −12 to switch between them. The "middle pin" of the switch is connected through a 27 kΩ resistor and a 100 kΩ potentiometer. The potentiometer is connected to the foil and GND to the silver wire. This permits controlling the current density and the anode/cathode assignment.

The target current density on the surface of the wire is between 1 and 5 mA/cm^2. The surface area of a cylinder is approximately $A = \pi dh$ (the end is negligible). For example, a 1" long piece of 0.005" wire has a surface area of 0.1 cm^2 and would need a resistance between 24 and 118 kΩ.

The anode and cathode should be alternated every 3-5 minutes for a few cycles and then the wire set as the anode for 10 minutes to develop a deep black AgCl coat.

APPENDIX E. EQUIPMENT SPECIFICATIONS

The following are relevant technical specifications for the various pieces of equipment used. Specifications and equipment listed are not intended to be exhaustive.

Aurora 809B *in situ* Apparatus: 305 x 220 mm extruded aluminum; 3-axis manipulator for muscle lever; 115 x 90 mm anodized aluminum platform with grid of M3 and 1.0 mm holes and 1/4" quick-connect fittings for temperature control.

Aurora 305C Muscle Lever: length=20 mm excursion, 1 μm resolution, 0.1% linearity over center 4 mm, 0.5% linearity over range, 1-to-99% step response=2.0 ms; force=0-5.0 N, 1.0 mN resolution, 0.2% linearity of force change, 1-to-99% step response=2 ms; outputs: length=1.0 mm/V, force=500.0 mN/V, dL/dt=200 mm/s/V, dF/dt=100.0 N/s/V; weight=1 kg.

Axon Digidata 1440A: sixteen 16-bit ±10V analog inputs (Z=1 MΩ), four 16-bit ±10V analog outputs (Z<0.1 Ω), and sixteen TTL digital outputs; F_s=1-250,000 Hz; maximum aggregate throughput of 4 megasamples/s.

Axon Axopatch 200B: zero offset; capacitance compensation (slow & fast); modes: V-clamp, I-clamp, track, I=0; low-pass filter: 1, 2, 5, 10, 100 kHz.

Fisher IsoTemp 6200 R20F: cooling capacity=250 W; temperature stability=±0.05°C; temperature resolution=0.01°C; temperature range=−20-100°C; reservoir=3-6 L; pump=21 L/min.

Newport VH3648W-OPT Vibration Isolation Table: operating pressure=5-10 PSI.

Newport FC3648 Faraday Cage.

Sutter Instruments P-1000 Micropipette Puller: pulling parameters=ramp, heat, velocity, pull, time/delay, pressure.

VSS 300 Series Isoflurance Vaporizer: gas flow=200-15,000 mL/min; capacity=125 mL isoflurane; calibration=0.25%, 0.5-5.0% in 0.5% increments

World Precision Instruments 1B150F-4 Capillary Glass: outside diameter=1.5mm; inside diameter=0.84 mm; length=4"; includes Kwik-Fil filament; firepolished

World Precision Instruments Accupulser A310: event interval=100μ to 1000 s; event delay=10 μs to 100 s; pulse width=10 μs to 100 s; train duration=100 μs to 1000 s; pulse interval=20 μs to 100 s; Z_{out}<1 Ω; 5 V CMOS output sync; 10-15 V output monitor.

World Precision Instruments Stimulus Isolator A365: constant-current operation; sixteen 9 V alkaline batteries; optocoupler=2500 V, 10^{12} Ω to ground; output ranges=0.1, 1.0, 10 mA; rise time=6 μs; fall time=10 μs